Research Square

Preprints are preliminary reports that have not undergone peer review.
They should not be considered conclusive, used to inform clinical practice,
or referenced by the media as validated information.

BMPR1B in TAMs promoted Oral Squamous Cell Carcinoma via increasing SMAD1/EGR1/PD-L1/XBP-1 signaling induced M2 polarization

Zhizheng Zhuang
Affiliated Hospital of Hebei University
Mujing Li
Affiliated Hospital of Hebei University
Yingshun Yang
Hebei Eye Hospital
Fang Xu
Affiliated Hospital of Hebei University
Fan Wu
wufanxufang@sina.com
Affiliated Hospital of Hebei University

Research Article

Keywords: BMPR1B, SMAD1/EGR1/PD-L1/XBP-1 signaling, oral squamous cell carcinoma, M2 polarization

Posted Date: September 7th, 2026

DOI: https://doi.org/10.21203/rs.3.rs-10584793/v1

License: This work is licensed under a Creative Commons Attribution 4.0 International License.
Read Full License

Additional Declarations: No competing interests reported.

Abstract

Objective

To characterize the cellular composition and macrophage polarization landscape of the oral squamous cell carcinoma (OSCC) tumor microenvironment using single-cell transcriptomics and to elucidate how OSCC-derived exosomal BMPR2 activates BMPR1B in tumor-associated macrophages (TAMs), promoting M2 polarization and tumor progression via the SMAD1/EGR1/PD-L1/XBP-1 signaling pathway.

Methods

Single-cell RNA sequencing data were analyzed using UMAP, cell annotation, pseudotime trajectory, cell-cell communication, and virtual gene knockout analyses to investigate cellular heterogeneity and macrophage differentiation in the OSCC microenvironment. Key signaling molecules were validated through bioinformatics analyses. A subcutaneous xenograft mouse model was established with BMPR1B overexpression, EGR1 knockdown, PD-L1 overexpression, and XBP1 knockdown treatment groups. Human Ca9-22 OSCC cells were co-cultured with THP-1-derived macrophages under hypoxia following lentiviral transfection. Western blotting, flow cytometry, colony formation, and wound-healing assays evaluated signaling, proliferation, cell-cycle progression, and migration.

Results

Eight major cellular populations were identified within the OSCC microenvironment. TAMs displayed increased M2 polarization, greater developmental heterogeneity, and stronger intercellular interactions than those in normal tissues. Virtual knockout analysis identified the BMPR2/SMAD1/EGR1 pathway as a regulator of PD-L1 expression. Functional studies demonstrated that OSCC-derived exosomal BMPR2 activates BMPR1B in macrophages, induces M2 polarization, and activates the SMAD1/EGR1/PD-L1/XBP-1 signaling cascade, thereby enhancing S-phase progression, proliferation, migration, and invasion of Ca9-22 cells.

Conclusion

Exosomal BMPR2 promotes M2 macrophage polarization and OSCC progression through the BMPR1B/SMAD1/EGR1/PD-L1/XBP-1 axis, identifying this signaling pathway as a promising therapeutic target for OSCC.

Introduction

Oral squamous cell carcinoma (OSCC) is one of the most common malignant tumors in the world, and it has high incidence and mortality rates, seriously threatening human health[1]. Despite some progress in diagnosis and treatment of OSCC in recent times, prognosis is still poor, mainly due to the invasive nature of the tumor, its ability to metastasize and its resistance to current therapies. Thus, an in-depth study on the molecular mechanism of OSCC and the discovery of new therapeutic targets are of great significance for improving the prognosis of patients.

The tumor microenvironment (TME) is a key factor in the initiation, progression and metastasis of tumors[2]. Tumor-associated macrophages (TAMs) are a vital component of the TME and have received increasing attention for their role in tumor progression[3]. M2 polarization of TAMs has been shown to be closely associated with progression of various malignancies, including orophacial squamous cell carcinoma. However, the precise molecular mechanism of the M2 polarization of TAMs in orophacial squamous cell carcinoma remains to be fully elucidated, which hinders the development of therapeutic strategies targeting TAMs.

Bone morphogenetic protein receptor 1B (BMPR1B) is a major receptor in bone morphogenetic protein (BMP) signaling pathway and is critically involved in embryonic development, bone formation and cell differentiation[4, 5]. Accumulating evidence in recent years has shown that BMPR1B is abnormally expressed in various cancers and is involved in regulating tumor cell proliferation, migration and invasion. However, the source of BMPR1B activation in TAMs and its role in M2 polarization have not been well studied. In this study, we demonstrate that OSCC cells upregulate exosome biogenesis (CD9, TSG101) and package BMPR2 into exosomes, which are then delivered to TAMs. The exosomal BMPR2 forms a functional complex with BMPR1B on the macrophage surface, initiating downstream signaling. This study is specifically focused on whether this tumor-derived exosomal BMPR2-macrophage BMPR1B axis regulates M2 polarization to affect OSCC progression.

This study aims to explore the molecular mechanism by which OSCC-derived exosomal BMPR2 activates BMPR1B on TAMs, thereby driving M2 polarization and affecting OSCC cell activity. Here we used single-cell transcriptomics and bioinformatic analysis to characterize the protein expression profile of TAMs in OSCC. Then we built a subcutaneous xenograft tumor model in nude mice and observed the tumor growth by overexpression and knockdown of genes such as BMPR1B, EGR1, PD-L1 and XBP-1. In addition, in vitro experiments were performed to investigate the role of BMPR1B in proliferation, migration and cell cycle of Ca9-22 oral squamous cell carcinoma cells. In this study, for the first time, the trans-cellular mechanism by which OSCC-derived exosomal BMPR2 activates BMPR1B on TAMs to drive M2 polarization through the SMAD1/EGR1/PD-L1/XBP-1 signaling axis was demonstrated, which opened up new ideas and ways for cancer therapy.

1 Materials and Methods

1.1 Cells and Materials

Human oral squamous cell carcinoma Ca9-22 cells were purchased from Guangzhou Genio Biotechnology Co., Ltd. THP-1 cells were obtained from the Cell Bank of the Shanghai Institute of Cell Biology, Chinese Academy of Sciences. Forty-five healthy, specific-pathogen-free (SPF) male BALB/c-nu nude mice, aged 6–8 weeks and weighing 16–20 g, were obtained from Henan Sikebasi Biotechnology Co., Ltd. (Laboratory Animal Production License No.: SCXK (Anhui) 2022-0018). The experimental animals were housed on a free-water diet. The animal facility was maintained at a constant temperature of 24°C and 60% relative humidity. Fetal bovine serum (164210-50) was purchased from Procell. RPMI-1640 medium, DMEM medium, penicillin-streptomycin (10,000 U/mL), serum-free medium (SFM), Lipofectamine™ 3000 transfection reagent, and dimethyl sulfoxide (DMSO) were all purchased from Thermo Fisher Scientific. The SMAD1 inhibitor Zilurgisertib and the EGR1 inhibitor EGR-1-IN-1 were purchased from MedChemExpress (MCE). The following antibodies were used: phosphorylated BMPR1B (1:1000), phosphorylated SMAD1 (1:1000), phosphorylated SMAD2/3 (1:1000), EGR1 (1:1000), PD-L1 (1:1000), XBP-1 (1:1000), and GAPDH (1:10,000) (all purchased from Abcam). Interleukin-10 (IL-10) and arginase-1 enzyme-linked immunosorbent assay (ELISA) kits were purchased from Jiangsu Meimian Industrial Co., Ltd. Total RNA extraction kits were purchased from Beijing Lanjieke Technology Co., Ltd. Hifair® II qPCR-specific first-strand cDNA synthesis master mix was purchased from Yeosen Biotechnology (Shanghai) Co., Ltd. Lentiviral vectors for BMPR1B overexpression, EGR1 knockdown, PDL1 overexpression, XBP1 knockdown, and SMAD2/3 overexpression were purchased from Guangzhou Bosa Gene Biotechnology Co., Ltd.

1.2 Bioinformatics Analysis

Download the OSCC-related data set GSE9844 from the GEO database. This data set consists of gene expression profiles of 12 healthy controls and 26 patients with oral squamous cell carcinoma. Raw microarray data were processed with the Robust Multiple Array Mean (RMA) method for background correction, normalization and probe aggregation. The Combat method was then applied to correct for batch effects in the processed expression matrix. Differential expression analysis was performed on the corrected data using the limma package. Differentially expressed genes (DEGs) were identified as those with |log2 fold change| > 1 and adjusted p-value < 0.05. P-values were adjusted for multiple testing using the Benjamini-Hochberg procedure. To better understand the biological functions of DEGs, Gene Ontology (GO) and Kyoto Encyclopedia of Genes and Genomes (KEGG) pathway enrichment analyses were conducted using the ClusterProfiler package. GO analysis consisted of three major categories, Cell Component (CC), Molecular Function (MF) and Biological Process (BP). KEGG analysis of differentially expressed genes was performed to identify enriched key signaling and metabolic pathways. Additionally, predefined gene sets closely associated with oral squamous cell carcinoma (including BMPR2, BMPR1B, SMAD1, SMAD2, SMAD3, EGR1, TGFβ1, PDL1 (CD274), PD1 (PDCD1), XBP1, ERS, IRE1∂ (ERN1), IL10, CD206 (MRC1), ARG1, CTSL, CTSB, CTSS, and IL4R). Spearman's correlation analysis was conducted to assess the relationship of their expression levels and to investigate the potential synergistic or antagonistic interaction patterns among these genes in OSCC. Finally, the results of the differential expression analysis were visualized using the ggplot2 package. The bioinformatic analyses provide critical clues and theoretical basis for elucidation of the molecular mechanisms of OSCC and provide

guidance for the subsequent experimental validation. In this study, we downloaded the transcriptomic sequencing data and the corresponding clinical follow-up information of the head and neck squamous cell carcinoma (HNSC) cohort from the database of The Cancer Genome Atlas (TCGA). The data for quantification of gene expression processed by the STAR workflow were downloaded with R language TCGAbiolinks package (version 2.26.0) and the expression levels of the BMPR1B gene in transcripts per million (TPM) were extracted. Simultaneously, GDCquery_clinic function was used to obtain the patients' clinical and pathological parameters, including age, sex, AJCC pathological stage and survival status (vital status, time to death and time to last follow-up). Only primary tumor samples with complete survival data and overall survival (OS) > 0 were included, resulting in 518 cases for the final analysis.

Overall survival was defined as the time from the initial diagnosis to death from any causes or the last follow up. To investigate the effect of the expression levels of BMPR1B on prognosis, the optimal expression cutoff based on the minimum P-value principle was identified by using the $surv_cutp\oint$ function of the $surv\ \min\ er$ package, and the patients were separated into high-expression and low-expression groups. Survival curves for both groups were plotted using the Kaplan–Meier method, and the log-rank test was used to compare differences between groups. Univariate and multivariate Cox proportional hazards regression models were used to evaluate the independent effect of BMPR1B expression grouping on overall survival, with adjustment for confounding factors, including age (continuous variable), sex (male/female), and pathological stage (stage I/II vs. stage III/IV). All statistical tests were two-sided and a P-value of less than 0.05 was considered statistically significant. Data were analyzed and graphically represented using R software (version 4.5.1).

1.3 Single-Cell Transcriptome Analysis

In this work, we report a systematic analysis of single-cell transcriptome data available in public databases. The scRNA-seq data were downloaded from Gene Expression Omnibus (GEO) (accession number: GSM5258385, GSM6258251). This dataset contains single-cell expression profiles of oral squamous cell carcinoma and corresponding normal tissues. Downloaded data were pre-processed expression matrices. To ensure the accuracy of subsequent analyses, data standardization, batch effect correction and dimensionality reduction were performed using Seurat v4.0. The oral squamous cell carcinoma cells were annotated and divided into subpopulations by integrating the SingleR database and known marker genes. FindMarkers was used to identify the differential genes between the oral squamous cell carcinoma group and the control group. To identify key signaling pathways, GO and KEGG enrichment analyses were performed by clusterProfiler. In this study, the score of apoptosis was calculated based on the pathological status of oral squamous cell carcinoma cells by a series of characteristic genes via the AddModuleScore. The difference of the score between the oral squamous cell carcinoma group and the normal group was evaluated by violin plots and UMAP visualization. The cellular stemness and differentiation levels were evaluated using the CytoTRACE algorithm to quantify the changes in cellular differentiation potential under different conditions. The effects of signal transduction and gene knockout were simulated by the computational biology methods. Cell state

transition diagrams were generated by Monocle 3, and pseudo-time analysis was performed to reveal the dynamic evolution trajectory of oral squamous cell carcinoma cells from a quiescent to a fibrotic phenotype. Finally, intercellular communication network was constructed by CellChat toolkit. Based on the ligand-receptor interaction databases, we visualized the interaction mode between oral squamous cell carcinoma cells as senders and receivers, and compared the difference in communication intensity and ligand-receptor pathways between oral squamous cell carcinoma and normal states.

1.4 Cell Line Culture and Grouping

Ca9-22 cells were cultured in DMEM medium containing 10% fetal bovine serum, 100 U/mL penicillin, and 100 μg/mL streptomycin. THP-1 cells were cultured in RPMI-1640 medium. THP-1 cells in the logarithmic growth phase were seeded at a density of 1×10^6 cells/mL in 6-well plates. Phorbol myristate acid ester (PMA) was added to each well at a final concentration of 100 ng/mL, and the cells were cultured under standard conditions for 48 hours to induce their differentiation into adherent macrophages. Upon completion of induction, the PMA-containing medium was discarded, and the cells were gently washed twice with PBS. Fresh RPMI-1640 medium was added, and the cells were allowed to stand for an additional 24 hours to fully recover and stabilize into the macrophage phenotype. Verification via CD11b and CD68 immunofluorescence staining showed a post-induction positivity rate > 90%, confirming successful differentiation into macrophages. This macrophage model was used in subsequent experiments to simulate tumor-associated macrophages (TAMs). Replace the medium after the cells have adhered.

1.4.1 Isolation and characterization of OSCC-derived exosomes

To investigate whether OSCC cells activate BMPR1B in macrophages via exosome-mediated delivery of BMPR2, exosomes were isolated from the culture supernatant of Ca9-22 cells. Briefly, Ca9-22 cells were cultured in exosome-depleted medium (DMEM containing 10% exosome-free FBS, prepared by ultracentrifugation at 100,000 × g for 16 h) for 48 h. The conditioned medium was collected and subjected to differential centrifugation: 300 × g for 10 min to remove cells, 2,000 × g for 20 min to remove debris, and 10,000 × g for 30 min to remove large vesicles. The supernatant was then ultracentrifuged at 100,000 × g for 70 min. The exosome pellet was washed once with PBS and ultracentrifuged again at 100,000 × g for 70 min. The final pellet was resuspended in PBS and quantified by BCA assay. Exosome markers CD9 and TSG101, as well as BMPR2, were detected by Western blotting. For transmission electron microscopy (TEM), exosomes were adsorbed onto formvar/carbon-coated grids and negatively stained with 2% uranyl acetate for morphological observation.

1.4.2 Knockdown of BMPR2 in Ca9-22 cells

To confirm the role of tumor-derived BMPR2 in exosome-mediated macrophage activation, BMPR2 expression was transiently knocked down in Ca9-22 cells using siRNA. Ca9-22 cells at 50–60% confluence were transfected with BMPR2-specific siRNA (si-BMPR2) or negative control siRNA (si-NC)

using Lipofectamine™ 3000 according to the manufacturer's protocol. At 48 h post-transfection, the culture medium was replaced with exosome-depleted medium, and the cells were cultured for an additional 48 h. Exosomes were then isolated from the supernatant as described above. Knockdown efficiency was verified by qPCR and Western blotting.

1.4.3 Exosome treatment of THP-1-derived macrophages

THP-1-derived macrophages (differentiated as described above) were seeded in 6-well plates and treated with 20 μg/mL of exosomes isolated from Ca9-22 cells (Exo-siNC or Exo-siBMPR2) or an equal volume of PBS as control. After 24 h of treatment, the cells were washed and lysed for Western blot analysis of p-BMPR1B, p-SMAD1, p-SMAD2/3 and downstream targets, or subjected to RNA extraction for qPCR analysis of M2 polarization markers. This experimental set-up was performed independently of the lentiviral overexpression/knockdown groups to specifically validate the trans-cellular signaling axis from tumor-derived exosomal BMPR2 to macrophage BMPR1B. THP-1-derived macrophages in the logarithmic phase were divided into the following groups: NC group, BMPR1B-OE group, BMPR1B-OE + Zilurgisertib group, BMPR1B-OE + Zilurgisertib + SMAD2/3-OE group, BMPR1B-OE + Zilurgisertib + SMAD2/3-OE + IN-1 group, BMPR1B-OE + Zilurgisertib + SMAD2/3-OE + IN-1 + PDL1-OE group, and BMPR1B-OE + Zilurgisertib + SMAD2/3-OE + IN-1 + PDL1-OE + XBP1-KD group. Stable overexpression or knockdown cell models of BMPR1B, EGR1, PDL1, XBP1, SMAD2/3, and their empty vector (ev) controls were established in THP-1 cells via lentiviral transduction. To determine the optimal working concentrations of Zilurgisertib (SMAD1 inhibitor) and EGR-1-IN-1 (EGR1 inhibitor), concentration gradients were established for screening. Zilurgisertib concentrations were set at 0 (NC), 1, 2.5, 5, and 10 μM; EGR-1-IN-1 concentrations were set at 0 (NC), 1, 5, 10, and 20 μM. After treating THP-1-derived macrophages with each concentration, the mRNA expression levels of downstream target genes (SMAD1 downstream reporter genes and EGR1 downstream target genes) were detected via qPCR. The lowest concentration that exhibited the most significant inhibitory effect without significant cytotoxicity was selected as the working concentration for subsequent experiments. Based on the screening results, 5 μM was selected for Zilurgisertib and 10 μM for EGR-1-IN-1.

An indirect co-culture system was established when both Ca9-22 cells and THP-1-derived macrophages were in the logarithmic growth phase. THP-1-derived macrophages were seeded on the bottom of a 6-well plate, and Ca9-22 cells were seeded in a Transwell insert with a pore size of 0.4 μm, which was placed inside the 6-well plate, allowing the two cell types to share the culture medium while remaining physically separated. The co-culture system was incubated at 37°C in a humidified incubator containing 1% O_2, 5% CO_2, and 94% N_2. Cells in logarithmic growth phase were selected and fresh medium was replaced the night before harvesting of the cells (Ca9-22). The cells were then trypsinized and re-suspended in serum-free medium to create a cell suspension. The cell suspension was diluted with high-concentration Matrigel at a ratio of 1:1 on an ice bath (4°C) to a final cell suspension concentration of 4 × 10 7 cells/mL. Cell grouping and treatment were randomized, and subsequent assessments of cell proliferation, migration, invasion, and cell cycle were conducted in a blinded manner; neither the experimenters nor the data analysts were aware of the group assignments.

Direct contact co-culture system: To compare the effects of direct contact between TAMs and OSCC cells on tumor cell function, a direct co-culture group was established. THP-1-derived macrophages and Ca9-22 cells were mixed in a 1:1 ratio and seeded into 6-well plates at a total density of 2×10^5 cells/well. The co-culture system was incubated in a humidified incubator containing 1% O_2, 5% CO_2, and 94% N_2 at 37°C for 48 hours. Upon completion of the co-culture, the two cell types were separated using a differential digestion method (shorter digestion time for Ca9-22 cells and longer digestion time for THP-1-derived macrophages), and the Ca9-22 cells were collected for subsequent clonogenic assays and Transwell experiments. The group design for direct co-culture was consistent with that of indirect co-culture, including: the NC group, the BMPR1B-OE group, the BMPR1B-OE+EGR1-KD group, the BMPR1B-OE+EGR1-KD+PDL1-OE group, and the BMPR1B-OE+EGR1-KD+PDL1-OE+XBP1-KD group.

Separation of OSCC cells from direct co-culture:

After the direct co-culture period, the mixed cell population was detached using 0.25% trypsin-EDTA and centrifuged at 300 × g for 5 minutes. The cell pellet was resuspended in PBS containing 0.5% bovine serum albumin (BSA) and 2 mM EDTA to prepare a single-cell suspension. To specifically isolate Ca9-22 cells, anti-EpCAM (CD326) MicroBeads (Miltenyi Biotec) were used according to the manufacturer's instructions. Briefly, cells were incubated with the MicroBeads at 4°C for 15 minutes, washed, and then applied to LS columns placed in a magnetic field. The labeled Ca9-22 cells retained in the column were eluted with the provided buffer after removing the column from the magnet. The purity of the isolated Ca9-22 cells was verified by flow cytometry, and these cells were then subjected to subsequent functional assays (colony formation, Transwell, etc.).

1.5 Establishment of the Nude Mouse Model and Grouping

After inducing anesthesia with 3% isoflurane, anesthesia was maintained with 1.5% isoflurane, and the cell suspension was injected subcutaneously into the left axilla of the nude mice. During inoculation, the needle depth was maintained at approximately 1 cm below the skin surface to minimize leakage of the cell suspension after injection. The injection site should be shallower than the needle length to avoid penetrating the skin or muscle layers. The inoculation procedure must be completed within 1 hour. The 72 nude mice with subcutaneous xenografts were divided into the following groups (9 mice per group): NC group, BMPR1B-OE group, BMPR1B-OE+EGR1-NC group, BMPR1B-OE+EGR1-KD group, BMPR1B-OE+EGR1-KD+PDL1-NC group, BMPR1B-OE+EGR1-KD+PDL1-OE group, BMPR1B-OE+EGR1-KD+PDL1-OE + XBP-1-NC group, and BMPR1B-OE+EGR1-KD+PDL1-OE + XBP-1-KD group. The mice were housed in the animal facility, and tumor volumes were measured on days 7, 14, and 21 to plot growth curves. The condition of the nude mice, mortality, and tumor growth were monitored daily. Tumor volume measurements and data recording were performed in a blinded manner, meaning the personnel conducting the measurements were unaware of the animal group assignments. On day 21, the nude mice were anesthetized by inhalation of isoflurane and transferred to induction chambers after measurement of tumor volume. Isoflurane concentration was kept at 3% and oxygen flow rate was 1 L/min. Induction continued for about 2–3 min until the mice’s breathing was significantly suppressed and the righting reflex was absent. After confirming the depth of anesthesia was sufficient, the mice

were transferred to a euthanasia chamber and exposed to carbon dioxide (CO2) at a flow rate of 20%-30% of the chamber volume per minute for a minimum of 5 minutes. Death was confirmed by cervical dislocation after the mice stopped breathing entirely and their heartbeats stopped. All animal carcasses were collected and sent to a designated locati0n for proper disposal. The entire euthanasia procedure was conducted in accordance with the AVMA Guidelines for the Euthanasia of Animals and protocol approved by the institutional animal ethics committee. Mice were provided food and water ad libitum during the experiment. The animal facility was maintained at a temperature of 24°C and relative humidity of 60%. Sample size was determined by preliminary experiments and power analysis. We used a one-way ANOVA design with an assumed large effect size (Cohen's f = 0.5) for the primary outcome (tumor volume) between groups, with α = 0.05 and statistical power (1-β) = 0.8, requiring a minimum of 7 mice per group. The sample size was increased to 9 mice per group (72 mice total) to account for the possible technical failure or animal attrition during the 21-day experimental period. All procedures were conducted in accordance with relevant guidelines and regulations, adhering to the 3Rs principles and the ARRIVE guidelines.

1.6 Western Blotting

Total protein was extracted from cells in each group, and protein concentration was determined using the Bradford method. A 50 μg protein sample was separated by 12% SDS-PAGE for 1.5 hours, followed by protein transfer to a PVDF membrane. The membrane was blocked with 1% bovine serum albumin overnight, then incubated with the corresponding primary antibody at 37°C for 2 hours. The primary antibodies used are as follows: Rabbit anti-human SMAD1 (total protein, catalog number ab170872, dilution 1:1000, Abcam); Rabbit anti-human SMAD2/3 (catalog number ab202445, dilution 1:1000, Abcam); Rabbit anti-human phosphorylated BMPR1B (p-BMPR1B, catalog number ab229400, dilution ratio 1:1000, Abcam); Rabbit anti-human phosphorylated SMAD1 (p-SMAD1, catalog number ab384800, dilution ratio 1:1000, Abcam); Rabbit anti-human phosphorylated SMAD2/3 (p-SMAD2/3, catalog number ab278844, dilution ratio 1:1000, Abcam); Rabbit anti-human EGR1 (catalog number ab226121, dilution ratio 1:1000, Abcam); Rabbit anti-human PD-L1 (catalog number ab263720, dilution ratio 1:1000, Abcam); Rabbit anti-human XBP-1 (specifically recognizes the splice variant sXBP-1, catalog number ab207528, dilution ratio 1:1000, Abcam); Rabbit anti-human CD9 (catalog number ab236630, dilution ratio 1:1000, Abcam); Rabbit anti-human TSG101 (catalog number ab125011, dilution ratio 1:1000, Abcam); Rabbit anti-human BMPR2 (catalog number ab281127, dilution ratio 1:1000, Abcam); mouse anti-human GAPDH (catalog number ab8245, dilution ratio 1:10,000, Abcam). After washing with TBST, incubate at 37°C with the corresponding HRP-labeled secondary antibodies (goat anti-rabbit IgG H&L, catalog number ab205718, dilution ratio 1:5000; goat anti-mouse IgG H&L, catalog number ab205719, dilution ratio 1:5000) at 37°C for 1 hour, followed by washing with TBST. Protein bands were visualized using the ECL chemiluminescence method, and band gray values were analyzed using ImageJ software. This experiment was repeated three times. Phosphorylation specificity was confirmed via λ-phosphatase treatment. Procedure: Take equal volumes of protein lysate, add λ-phosphatase (400 U/mL) and $MnCl_2$ (1 mM), incubate at 30°C for 30 minutes, and then perform Western blot analysis. If the signal for the p-

BMPR1B band completely disappears or is significantly reduced, this confirms that the antibody recognizes a phosphorylated epitope.

1.7 Quantitative Real-Time PCR (qPCR) for the Detection of Arginase-1, IL-10, Cathepsin B, and Cathepsin S Expression

Total RNA was extracted from cells using a total RNA isolation kit according to manufacturer's protocol. The Hifair® II 1st Strand cDNA Synthesis Supermix Kit (for qPCR) was used for reverse transcription and amplification reactions according to the manufacturer's instructions.

Primer Efficiency Validation: The amplification efficiency of each primer pair was validated using the standard curve method. The cDNA template was serially diluted in a 5-fold gradient (1:1, 1:5, 1:25, 1:125, 1:625). qPCR amplification was performed using templates at each dilution, and a standard curve was plotted with Ct values on the y-axis and the logarithm of the template dilution factor on the x-axis. The formula for calculating primer amplification efficiency (E) is E = (10^(-1/slope) − 1) × 100%. The primer amplification efficiencies used in this study ranged from 90% to 110%, and the correlation coefficients (R^2) of the standard curves were all greater than 0.99, indicating that the primers possess good amplification efficiency.

Validation of reference gene stability: The geNorm software was used to assess the expression stability of candidate internal reference genes (β-actin, GAPDH, 18S rRNA) under experimental conditions. Based on the mean stability value (M value), β-actin had the lowest M value (M = 0.32), followed by GAPDH (M = 0.45), while 18S rRNA had an M value of 0.68. Therefore, β-actin was selected as the internal control gene for this experiment.

Verification of lentiviral infection efficiency: The mRNA expression levels of the target gene in cell models with gene overexpression or knockdown were detected via qPCR to verify lentiviral infection efficiency. The results showed that, compared with the NC group, BMPR1B mRNA expression levels in the BMPR1B-OE group increased to 4.21 ± 0.35-fold ($P < 0.001$); EGR1 mRNA expression levels in the EGR1-KD group decreased to 0.23 ± 0.04-fold of the NC group ($P < 0.001$); in the PDL1-OE group, PD-L1 mRNA expression levels increased to 3.85 ± 0.31-fold ($P < 0.001$); in the XBP1-KD group, XBP-1 mRNA expression levels decreased to 0.19 ± 0.03-fold that of the NC group ($P < 0.001$); In the SMAD2/3-OE group, SMAD2/3 mRNA expression levels increased to 4.02 ± 0.28-fold ($P < 0.001$). These results indicate that the construction of each lentiviral transduction cell model was successful and can be used for subsequent experiments.

The qPCR reaction protocol was as follows: 5-minute pre-denaturation at 95°C; denature at 95°C for 10 seconds, anneal at 60°C for 30 seconds, and extend at 72°C for 30 seconds, for a total of 40 cycles; followed by melting curve analysis (from 65°C to 95°C, with fluorescence signals read every 0.5°C). Results were calculated and analyzed using the 2^(-ΔΔCT) method. β-actin was used as the internal control gene.

Primer sequences:

Arginase-1: Forward Primer (F): 5’-CTCCAAGCCAAAGTCCTTAGAG-3’; Reverse Primer (R): 5’-AGGAGCTGTCATTAGGGACATC-3’.

Interleukin-10 (IL-10): Forward Primer (F): 5’-GCTGGACAACATACTGCTAACCG-3’; Reverse Primer (R): 5’-GGAAGACCTCGGTAGCAGCTAT-3’.

Cathepsin B: Forward Primer (F): 5’-CGGGAAGTCACAGAGGGTAT-3’; Reverse Primer (R): 5’-CAGGGTACACGGTGTGGAAT-3’.

Cathepsin S: Forward Primer (F): 5’-GCTGGTGGTGCTGTTCATCT-3’; Reverse Primer (R): 5’-CAGGACAGGGTGTGGAAGTC-3’.

β-actin (internal reference): Forward Primer (F): 5’-CATGTACGTTGCTATCCAGGC-3’; Reverse Primer (R): 5’-CTCCTTAATGTCACGCACGAT-3’.

CD206 (MRC1): Forward Primer (F): 5'-CGGTGGAGGTGATGGTTCTC-3'; Reverse Primer (R): 5'-GCTGTTCCAGTTGCGGTAGT-3'.

CD163: Forward Primer (F): 5'-GGGGTGGAGTGCTCTGTGTA-3'; Reverse Primer (R): 5'-CAGCATCCTTGAGGTCCAGT-3'.

IL-4R: Forward Primer (F): 5'-GCTGGAGAACCTGTGGAAGT-3'; Reverse Primer (R): 5'-TGCACACGGTAGTTCCTGTT-3'.

TGF-β: Forward Primer (F): 5'-GGCCAGATCCTGTCCAAGC-3'; Reverse Primer (R): 5'-GTGGGTTTCCACCATTAGCAC-3'.

1.8 ELISA Assay

Cell supernatants were collected 24 hours after drug treatment. The concentrations of arginase-1 and IL-10 were determined according to the instructions of the corresponding ELISA kits. The optical density (D(λ)) values of the samples were measured using a microplate reader, and the concentrations of the target factors were calculated based on these values.

1.9 Flow Cytometry for Cell Cycle Analysis

Ca9-22 cells in the logarithmic growth phase were seeded into a 6-well plate at a density of 3×10^5 cells per well. After the cells had adhered, the culture medium was replaced following the procedure described in Section 1.4. After 48 hours of culture, collect the cells, wash them with PBS, and fix them overnight with 70% ethanol at 4°C. Subsequently, wash the cells with PBS, resuspend them in 0.5 mL of propidium iodide (PI) staining solution, incubate for 30 minutes in a 37°C water bath protected from light, and then store in the dark at 4°C. Analyze the cell cycle distribution using a flow cytometer.

1.10 Colony Formation Assay

Ca9-22 cells in logarithmic growth phase were suspended into a single cell suspension at a density of 1.5×103 cells/mL. Add 2 mL of the suspension to each well of a 6-well plate and place the plate in a cell culture incubator. When the cells are fully adhered, treat with drug as described in Section 1.4. Cell cultures were maintained for 7–14 days, with medium changes every 3 days. Cells were stained with crystal violet after culture and then the formation of colonies was observed and photographed.

1.11 Wound Healing (Scratch) Assay

Migration ability of Ca9-22 cells was evaluated by wound healing assay. A marker was used to draw uniform horizontal lines on the bottom of a 6-well plate so that at least 3 lines intersected in each well. Plate approximately 3 × 10^5 cells/well. Culture the cells in DMEM medium without fetal bovine serum (FBS) at 37°C in 5% CO2 incubator. After cells have adhered stably, scratch with a tip of a 200 μL pipette in a direction perpendicular to the horizontal lines that are drawn on the bottom of the plate, holding a constant initial scratch width (approximately 500 μm). Then cells migrate slowly from the edge of the scratch to the center to close the gap. After the scratching, wash the detached cells away 3 times with PBS, and continue the culture under serum-free conditions. Image at 0 hours and 48 hours. Measure the scratch width by ImageJ software.

1.12 Transwell Assay

Cell invasion was evaluated using a Matrigel-coated Transwell assay. The upper surface of the Transwell membrane was precoated with Matrigel and allowed to air-dry before use according to the manufacturer's instructions. Cells from each experimental group were initially cultured in 6-well plates at a density of 1×10^6 cells/well. Upon reaching approximately 80% confluence, the culture medium was replaced with serum-free medium, and the cells were incubated overnight.

Cells were harvested, resuspended in serum-free medium at a concentration of 1×10^5 cells/mL, and 100 μL of the cell suspension was added to the upper chamber of each Transwell insert. The lower chamber was filled with 600 μL of RPMI-1640 medium supplemented with 10% fetal bovine serum (FBS) as a chemoattractant. Following overnight incubation at 37°C in a humidified atmosphere containing 5% CO_2, the Transwell inserts were removed. Non-invading cells remaining on the upper surface of the membrane were gently removed using a cotton swab. Cells that had invaded through the membrane to the lower surface were fixed with methanol for 30 minutes, stained with 0.1% crystal violet, and examined under a light microscope. Invaded cells were counted in randomly selected microscopic fields. Each experimental group was analyzed using six biological replicates.

Cell Migration Assay

Cell migration was assessed using a Transwell migration assay without Matrigel coating. Transwell inserts were placed into 24-well plates, and cells from each experimental group were harvested, counted, and seeded into the upper chamber in serum-free medium. The lower chamber was filled with 1 mL of

culture medium containing 20% fetal bovine serum (FBS) to establish a chemotactic gradient, ensuring that the medium covered the underside of the membrane without overflowing into the upper chamber.

The cells were incubated at 37°C in a humidified incubator with 5% CO_2 for 24 hours. After incubation, the Transwell inserts were removed, and non-migrated cells on the upper surface of the membrane were carefully removed using a cotton swab. The membranes were washed twice with phosphate-buffered saline (PBS), fixed with 4% paraformaldehyde for 15 minutes at room temperature, washed twice with PBS, and stained with crystal violet for 15 minutes. Excess stain was removed by washing the membranes three times with PBS.

Migrated cells attached to the underside of the membrane were observed and photographed using an inverted microscope. Images were acquired from five randomly selected fields per membrane, and quantitative analysis of migrated cells was performed using ImageJ software. Each experimental group was evaluated with three biological replicates.

1.13 Statistical Methods

Statistical analysis was performed using GraphPad Prism 9.0 software. Measurement data are expressed as mean ± standard deviation. Comparisons between two groups were performed using t-tests, and comparisons among multiple groups were performed using one-way analysis of variance (ANOVA). A p-value less than 0.05 ($P < 0.05$) was considered statistically significant.

2 Results

2.1 Single-Cell Transcriptomic Analysis of OSCC

Based on the preprocessing and analysis of dataset GSE9844, this study obtained the following important findings related to oral squamous cell carcinoma (OSCC): Firstly, we assessed the standardization effect of the data using box plots and examined the sample distribution after batch effect correction using PCA plots. The results indicated good data quality, suitable for subsequent analysis (Fig. 1A). Differential expression analysis using the limma package identified a total of 572 significantly differentially expressed genes (DEGs), including 260 upregulated genes and 312 downregulated genes (Fig. 1B). Notably, the BMPR2 gene was highly expressed in OSCC tissues, suggesting it may play an important role in the tumor's development and progression (Fig. 1C). GO functional enrichment analysis performed with ClusterProfiler revealed that these DEGs were significantly enriched in multiple functional categories highly relevant to OSCC: In Cellular Components, genes were significantly enriched in structures such as the actin cytoskeleton, focal adhesion, and basal plasma membrane, which are closely related to malignant phenotypes like tumor cell migration, invasion, and loss of polarity. In Molecular Functions, DEGs were significantly enriched in functions related to extracellular matrix interaction and signal transduction. In Biological Processes, genes were significantly involved in processes such as epithelial cell proliferation, response to virus, and tissue remodeling,

directly linking to key pathological features of OSCC like abnormal cell proliferation, response to viral infection, and tumor microenvironment remodeling (Fig. 1D-F). KEGG pathway analysis further revealed that DEGs were significantly enriched in several known cancer-related signaling pathways, including the PI3K – Akt signaling pathway, Human papillomavirus infection, Focal adhesion, Relaxin signaling pathway, TNF signaling pathway, AGE–RAGE signaling pathway in diabetic complications, and the p53 signaling pathway. This enrichment result confirms, from a systems biology perspective, that the development and progression of OSCC involve dysregulation of multiple core pathways related to cell proliferation, survival, metabolism, inflammatory response, and maintenance of genomic stability (Fig. 1G-H). Based on Spearman correlation analysis, this study identified multiple gene pairs with significant positive correlations in OSCC samples. These relationships reveal molecular networks that may function synergistically in OSCC pathogenesis. Specific results are as follows:

XBP1 as a key hub, positively correlating with multiple immune and metabolism-related genes:

XBP1 correlated positively with CTSS, CTSB, and CTSL, suggesting functional linkage between endoplasmic reticulum stress and the lysosomal cysteine protease system in OSCC.XBP1 correlated positively with IL4R and IL10, indicating its potential involvement in regulating M2 macrophage polarization.XBP1 correlated positively with PDL1 and PD1, implying that the endoplasmic reticulum stress response may be related to the formation of an immunosuppressive tumor microenvironment.XBP1 correlated positively with ARG1 and CD206, further supporting its role in myeloid cell functional remodeling.XBP1 correlated positively with IRE1α, validating the sustained activation of this signaling axis in the unfolded protein response within OSCC.

High coordination within the BMP/TGF-β signaling pathway:

BMPR2 expression positively correlated with BMPR1B.BMPR1B positively correlated with SMAD1.SMAD1 positively correlated with SMAD2. SMAD2 and SMAD3 both positively correlated with EGR1 expression, and EGR1 in turn correlated with TGFβ1 expression. TGFβ1 formed a positive feedback loop with SMAD2 and SMAD3, collectively constituting a complete BMP/TGF-β-SMAD signal transduction and transcriptional regulatory network. Potential interaction between immune regulation and endoplasmic reticulum stress:EGR1 expression positively correlated with PDL1, suggesting this transcription factor may be involved in regulating immune checkpoint molecule expression.PDL1 correlated positively with PD1 and ERS (Endoplasmic Reticulum Stress) markers; PD1 also correlated with ERS expression, indicating a potentially mutually reinforcing mechanism between the immune checkpoint pathway and endoplasmic reticulum stress in OSCC. ERS markers positively correlated with IRE1α expression, further confirming the active state of the endoplasmic reticulum stress pathway in OSCC (Fig. 1I-J). In summary, these correlation analysis results systematically reveal potential synergistic regulatory relationships among multiple key pathways in OSCC—including BMP/TGF-β signaling, endoplasmic reticulum stress response, immune checkpoints, and tumor-associated protease systems—providing new clues for a deeper understanding of the molecular network in OSCC.

A: UMAP expression distribution of genes;

B: Violin plot of gene expression across cell types;

C: UMAP dimensionality reduction and clustering of cell types;

D: Heatmap of gene expression by cell type.

The UMAP dimensionality reduction visualization results show that all cells were clustered into 8 major cell clusters, representing various cell types in the tumor microenvironment. Based on the expression of classic marker genes, we identified these cell clusters as: epithelial cells (EPCAM+), basal cells (KRT5+/KRT17+), ciliated epithelial cells (FOXJ1+), activated T cells (CD3D+/CD8A+), monocytes (CD14+), macrophages (C1QA+/C1QB+), fibroblasts (DCN+/COL1A1+), and proliferating cells (MKI67+/TOP2A+) (Fig. 2A). Furthermore, we focused on the macrophage population and analyzed the expression of key functional marker genes. The results indicate that macrophages highly express the pan-macrophage markers CD68 and ADGRE1 (F4/80), as well as the colony-stimulating factor 1 receptor (CSF1R). Notably, we detected the expression of markers associated with pro-tumor phenotypes, such as VEGFA (vascular endothelial growth factor A) and the immune checkpoint molecule PD-L1, as well as proteins relevant to this study, in certain macrophage subpopulations (Fig. 2B). Further analysis of cell origin revealed that cells from tumor (Tumor) and normal (Normal) tissues exhibited a trend toward partial separation in the UMAP space, particularly within the epithelial and immune cell populations, indicating that tumorigenesis is accompanied by significant transcriptomic reprogramming (Fig. 2C). The UMAP plots for nCount_RNA and nFeature_RNA show that there are no significant batch effects in cell sequencing depth (nCount_RNA) or the number of detected genes (nFeature_RNA) across subpopulations, ensuring data reliability. Cell cycle analysis revealed that the “Proliferating cells” cluster consists primarily of cells in the S and G2/M phases, while the remaining cells are predominantly in the G1 phase, consistent with our cell annotation results (Figure. 2D–F).

A: Cell type UMAP plot

B: Expression of macrophage marker genes

C: Clustering UMAP plot

D: nCount_RNA UMAP plot

E: nFeature_RNA UMAP plot

F: Cell cycle UMAP plot;

To investigate key molecular events during tumorigenesis, we performed differential expression analysis between the tumor and normal groups. Volcano plot results revealed a large number of significantly differentially expressed genes in tumor tissues compared to normal tissues. Of these, genes including KRT76, TGM3 and CRNN were significantly down-regulated, and genes such as KRT19, ATP5E and

AKR1C3 were significantly up-regulated, indicating profound changes in keratinization and metabolism of tumor cells (Fig. 3A).

A: Volcano plot of differentially expressed genes

B: Bar chart of GO enrichment analysis

C: Bubble plot of KEGG enrichment analysis

D: Gene set enrichment analysis

E: Inter-group comparison of macrophage M2 polarisation scores

F: Violin plot comparison of macrophage M2 polarisation scores between the normal (Normal) and tumour (Tumour) groups

G: Box plot comparison of macrophage M2 polarisation scores between the normal (Normal) and tumour (Tumour) groups;

H–J: Results following virtual knockout of BMPR2, SMAD2 and EGR1.

GO analysis showed that up-regulated genes were significantly enriched in biological processes such as “cytoplasmic translation”, “mitochondrial ATP synthesis”, and “electron transport chain”, and cellular components such as “ribosomal subunits” and “ribosomes”. On the other hand, down-regulated genes were mainly enriched in pathways associated with normal epithelial cell function, such as “keratinization”, “epithelial cell differentiation”, and “skin development”. KEGG analysis also showed that pathways such as “ribosomes” and “oxidative phosphorylation” were significantly activated in tumor tissues, whereas pathways such as “keratinization” were suppressed (Fig. 3B, C).

Further GSEA analysis supported these findings. The results indicated significant enrichment of the “oxidative phosphorylation” (HALLMARK_OXIDATIVE_PHOSPHORYLATION) gene set of tumor tissues (NES > 0) and implied a change in the energy metabolism of tumor cells toward oxidative phosphorylation. Concurrently, the “downregulated KRAS signaling” (HALLMARK_KRAS_SIGNALING_DN) gene set was significantly negatively enriched in tumor tissues (NES < 0), suggesting that the KRAS signaling pathway is activated in tumors. Collectively, these results reveal extensive transcriptional reprogramming in tumor tissues, primarily involving key biological processes such as cell proliferation, energy metabolism, and signal transduction (Fig. 3D).

Given the critical role of macrophages in tumor immunity, we further analyzed their polarization status within the tumor microenvironment. UMAP plots revealed that cells with higher M2 polarization scores were predominantly concentrated in specific macrophage subpopulations, indicating significant heterogeneity in the functional state of macrophages (Fig. 2E). Comparison of macrophage polarization scores between normal and tumor tissues revealed that the M2 polarization score in the tumor group was significantly higher than that in the normal group (Wilcoxon test, P = 5.83e-04), suggesting that the

tumor microenvironment induces macrophage differentiation toward the M2 phenotype, which exhibits immunosuppressive and tumor-promoting functions. Box plots and violin plots further corroborated these findings, clearly demonstrating an overall increase in M2 polarization levels within the macrophage population in the tumor group (Fig. 3F, G). Collectively, these data suggest that the tumor microenvironment shifts the macrophage polarization balance towards the immunosuppressive M2 phenotype, which may facilitate tumor cell immune evasion and progression. The in silico knockdown of BMPR2 resulted in a significant reduction in its expression level (Log2FC = − 41.56), which validated the model's performance. Furthermore, the expression level of BMPR1B was significantly reduced (Log2FC = − 9.09). Following virtual knockout of SMAD2, its own expression level was significantly reduced (Log2FC = -36.31), and EGR1 expression was significantly reduced (Log2FC = -9.68). Following virtual knockout of EGR1, its own expression level was significantly reduced (Log2FC = -45.57), and the expression level of PD-L1 was significantly reduced (Log2FC = -7.63). This further validated the experimental results (Fig. 3H–J). Other results of the single-cell transcriptome analysis were provided in Supplementary File 1.

2.2 Prognostic Value of BMPR1B Expression in HNSC

An analysis of 518 samples from the TCGA-HNSC cohort revealed that the optimal cutoff value for BMPR1B expression, determined using the minimum P-value method, was 4.24 TPM. Based on this, patients were divided into a high-expression group (> 4.24) and a low-expression group (≤ 4.24). Kaplan–Meier survival curves indicated that overall survival was significantly shorter in the high-expression group compared to the low-expression group, with the survival curves showing a clear divergence (log-rank P = 0.017) (Fig. 4A). Univariate Cox regression analysis suggested that low expression was associated with a reduced risk of death (HR = 0.71, 95% CI: 0.53–0.94, P = 0.017) (Fig. 4B). After further adjustment for age, sex, and pathological stage in a multivariate Cox model, low BMPR1B expression remained independently associated with better survival (adjusted HR = 0.65, 95% CI: 0.49–0.87, P = 0.003). Additionally, advanced pathological stage (stage III/IV vs. stage I/II; HR = 1.98, 95% CI: 1.34–2.93, P < 0.001) and increasing age (HR = 1.02 per year, 95% CI: 1.01–1.04, P < 0.001) were also independent risk factors, whereas gender did not show statistical significance (P = 0.125) (Fig. 4C). These results indicate that elevated BMPR1B expression is an independent predictor of poor prognosis in HNSC patients.

A: Comparison of Kaplan–Meier overall survival curves between the high and low BMPR1B expression groups. The x-axis represents survival time (days), and the y-axis represents the probability of overall survival.

B: Forest plot of univariate Cox regression analysis showing the effect of BMPR1B expression levels on overall survival.

C: Time-dependent ROC analysis for predicting overall survival.

The predictive performance of BMPR1B expression was evaluated at 1, 3, and 5 years. The AUC values were 0.523 for 1-year, 0.533 for 3-year, and 0.500 for 5-year survival, indicating limited sensitivity and specificity.

2.3 BMPR1B signaling in TAMs promotes OSCC tumor growth via the EGR1/PD-L1/XBP-1 pathway

Compared with the NC group, tumor volume increased in the BMPR1B-OE group ($p = 0.008$); compared with the BMPR1B-OE group, tumor volume increased in the BMPR1B-OE+EGR1-NC group; Compared with the BMPR1B-OE+EGR1-NC group, tumor volume was reduced in the BMPR1B-OE+EGR1-KD group; compared with the BMPR1B-OE+EGR1-KD group, tumor volume was reduced in the BMPR1B-OE+EGR1-KD+PDL1-NC group; Compared with the BMPR1B-OE+EGR1-KD+PDL1-NC group, the BMPR1B-OE+EGR1-KD+PDL1-OE group showed an increase in tumor volume; Compared with the BMPR1B-OE+EGR1-KD+PDL1-OE group, the BMPR1B-OE+EGR1-KD+PDL1-OE + XBP-1-NC group showed an increase in tumor volume; Compared with the BMPR1B-OE+EGR1-KD+PDL1-OE + XBP-1-NC group, the BMPR1B-OE+EGR1-KD+PDL1-OE+XBP1-KD group showed a reduction in tumor volume (Fig. 5).

A: Representative images of subcutaneous tumors from the indicated groups: NC group, BMPR1B-OE group, BMPR1B-OE+EGR1-NC group, BMPR1B-OE+EGR1-KD group, BMPR1B-OE+EGR1-KD+PDL1-NC group, BMPR1B-OE+EGR1-KD+PDL1-OE group, BMPR1B-OE+EGR1-KD+PDL1-OE + XBP-1-NC group, and BMPR1B-OE+EGR1-KD+PDL1-OE + XBP-1-KD group.

B: Statistical analysis of tumor weight (g) in each group.

C: Tumor volume growth curves measured at indicated time points (Days 0, 7, 14, 21).

Data are presented as mean ± SD, n = 9 per group. $^{ns}p > 0.05$, $*p < 0.05$.

2.4 BMPR1B Induces M2 Polarisation

Compared with the NC group, p-BMPR1B, p-SMAD1, p-SMAD2/3, EGR1, PD-L1 and XBP-1s were all significantly elevated in the BMPR1B-OE group (Fig. 6A), whilst M2 polarisation-associated markers arginase-1, IL-10, cathepsin B, cathepsin S, CD206, CD163, IL-4R and TGF-β also showed an upward trend (Figs. 6B-D). Compared with the BMPR1B-OE group, there was no statistically significant difference in p-BMPR1B levels in the BMPR1B-OE+Zilurgisertib group, whilst expression levels of p-SMAD1, p-SMAD2/3, EGR1, PD-L1and XBP-1s were reduced, whilst arginase-1, IL-10, cathepsin B, cathepsin S, CD206, CD163, IL-4Rand TGF-β. Compared with the BMPR1B-OE+Zilurgisertib group, the BMPR1B-OE+Zilurgisertib+SMAD2/3-OE group showed no statistically significant differences in p-BMPR1B and p-SMAD1, whilst expression levels of p-SMAD2/3, EGR1, PD-L1and XBP-1s, whilst expression levels of arginase-1, IL-10, cathepsin B, cathepsin S, CD206, CD163, IL-4R and TGF-β. Compared with the BMPR1B-OE+Zilurgisertib+SMAD2/3-OE group, the BMPR1B-OE+Zilurgisertib+SMAD2/3-OE + IN-1 group showed no statistically significant differences in p-BMPR1B, p-SMAD1 and p-SMAD2/3, whilst EGR1, PD-L1 and XBP-1s, whilst expression levels of arginase-1, IL-10, cathepsin B, cathepsin S, CD206, CD163, IL-

4R and TGF-β. Compared with the BMPR1B-OE+Zilurgisertib+SMAD2/3-OE + IN-1 group, the BMPR1B-OE+Zilurgisertib+SMAD2/3-OE + IN-1 + PDL1-OE group showed no statistically significant differences in p-BMPR1B, p-SMAD1, p-SMAD2/3 and EGR1, whilst expression levels of PD-L1 and XBP-1s were elevated, and those of arginase-1, IL-10, cathepsin B, cathepsin S, CD206, CD163, IL-4R and TGF-β were all elevated. Compared with the BMPR1B-OE+Zilurgisertib+SMAD2/3-OE + IN-1 + PDL1-OE group, the BMPR1B-OE+Zilurgisertib+SMAD2/3-OE + IN-1 + PDL1-OE+XBP1-KD group showed no significant differences in p-BMPR1B, p-SMAD1, p-SMAD2/3, EGR1 and PD-L1, whilst XBP-1s expression was reduced, and arginase-1, IL-10, Cathepsin B, Cathepsin S, CD206, CD163, IL-4R and TGF-β.

A: Western blot detection of p-BMPR1B, p-SMAD1, p-SMAD2/3, EGR1, PD-L1, and XBP-1 expression in the following groups: NC group, BMPR1B-OE group, BMPR1B-OE+Zilurgisertib group, BMPR1B-OE+Zilurgisertib+SMAD2/3-OE group, BMPR1B-OE+Zilurgisertib+SMAD2/3-OE + IN-1 group, BMPR1B-OE+Zilurgisertib+SMAD2/3-OE + IN-1 + PDL1-OE group, and BMPR1B-OE+Zilurgisertib+SMAD2/3-OE + IN-1 + PDL1-OE+XBP1-KD group;

B: Q-PCR detection of arginase-1, IL-10, Cathepsin B and Cathepsin S levels in each group;

C: ELISA detection of arginase-1 and IL-10 levels in each group.

D: Q-PCR detection of CD206, CD163, IL-4R and TGF-β levels. Data are presented as mean ± SD, n = 3 per group. $^{ns}p > 0.05$, $*p < 0.05$.

2.5 OSCC-derived exosomes deliver BMPR2 to activate BMPR1B in TAMs, and BMPR1B regulates p-SMAD2/3 expression via SMAD1

To preliminarily investigate the potential mechanisms by which oral squamous cell carcinoma (OSCC) cells regulate tumour-associated macrophages (TAMs) via exosomes, this study used Western blot analysis to detect the protein expression levels of the exosome markers CD9, TSG101 and BMPR2 in normal oral cells and OSCC cells. The results showed that in the normal oral cell group, CD9, TSG101 and BMPR2 all exhibited weak positive expression; whereas in the oral squamous cell carcinoma group, the expression levels of all three were significantly upregulated (Fig. 7A). These findings suggest that OSCC cells may participate in intercellular signalling within the microenvironment by enhancing exosome biogenesis and BMPR2 loading. To directly test this, we isolated exosomes from Ca9-22 culture supernatant and treated THP-1-derived macrophages. Western blot confirmed that Ca9-22 exosomes contain BMPR2 protein. Upon exosome treatment, p-BMPR1B levels in recipient macrophages were significantly elevated compared to PBS-treated controls, and this effect was abrogated when exosomes were derived from BMPR2-knockdown Ca9-22 cells, demonstrating that tumor-derived exosomal BMPR2 is the upstream activator of macrophage BMPR1B.

A: Western blot detection of CD9, TSG101, and BMPR2 expression in NC (normal oral cells) and OSCC (Ca9-22 cells) groups, and BMPR2 protein in exosomes isolated from Ca9-22 cell culture supernatant

with or without prior BMPR2 knockdown (si-BMPR2) compared to si-NC control. Data are presented as mean ± SD, n = 3 per group.

B: Western blot detection of p-SMAD1, t-SMAD1, p-SMAD2/3, and t-SMAD2/3 expression in the following groups: NC group, BMPR1B-OE group, BMPR1B-KD group, BMPR1B-OE+SMAD1-KD group, and BMPR1B-OE+SMAD1-OE group. Data are presented as mean ± SD, n = 3 per group. $^{ns}p > 0.05$, $*p < 0.05$.

Having established that OSCC-derived exosomal BMPR2 activates macrophage BMPR1B, we next verified whether BMPR1B regulates the phosphorylation levels of downstream p-SMAD2/3 via SMAD1. To this end, we established BMPR1B and SMAD1 overexpression and knockdown models in THP-1 cells differentiated into macrophages (mimicking tumour-associated macrophages, TAMs) by PMA induction, and detected the protein expression levels of p-SMAD1, total SMAD1, p-SMAD2/3 and total SMAD2/3. The results showed that in the NC group, both p-SMAD1 and p-SMAD2/3 were positively expressed, whilst total SMAD1 and total SMAD2/3 remained stable. Compared with the NC group, the BMPR1B-OE group showed significantly upregulated expression levels of p-SMAD1 and p-SMAD2/3, whilst there were no significant changes in the expression levels of total SMAD1 and total SMAD2/3; and the ratios of p-SMAD1/t-SMAD1 and p-SMAD2/3/t-SMAD2/3 were both significantly elevated. In the BMPR1B-KD group, the expression levels of p-SMAD1 and p-SMAD2/3 were both significantly downregulated, whilst there were no significant changes in the expression levels of total SMAD1 and total SMAD2/3; the phosphorylated/total protein ratios were significantly reduced. Compared with the BMPR1B-OE group, the BMPR1B-OE+SMAD1-KD group showed significantly reduced expression of p-SMAD1 and a corresponding decrease in p-SMAD2/3 expression, whilst total SMAD1 expression levels were also reduced. whilst total SMAD2/3 expression showed no significant change, and the p-SMAD2/3/t-SMAD2/3 ratio decreased; In the BMPR1B-OE+SMAD1-OE group, p-SMAD1 expression was further enhanced, p-SMAD2/3 expression was also simultaneously enhanced, total SMAD1 expression levels increased, total SMAD2/3 expression showed no significant change, and the p-SMAD2/3/t-SMAD2/3 ratio increased (Fig. 7B).

These results indicate that BMPR1B influences the phosphorylation levels of p-SMAD2/3 by regulating the phosphorylation levels of SMAD1; furthermore, this regulatory effect is not achieved by altering the expression of total SMAD proteins, but rather by directly influencing the phosphorylation cascade, thereby providing direct experimental evidence for the functional activation of the BMPR1B/SMAD1/SMAD2/3 signalling cascade.

2.6 BMPR1B promotes OSCC cell proliferation, migration, and invasion via the SMAD1/EGR1/PD-L1/XBP-1 axis (Indirect co-culture)

To evaluate the biological function of the BMPR1B signaling axis in TAMs on OSCC cells, an indirect co-culture system was established. The effect of the SMAD1/EGR1/PD-L1/XBP-1 signaling pathway was evaluated using specific inhibitors and gene overexpression/knockdown. Compared with the NC group,

the BMPR1B-OE group exhibited significantly increased S-phase proportions, colony-forming units, migratory capacity and invasive capacity in Ca9-22 cells. Compared with the BMPR1B-OE group, the proportion of Ca9-22 cells in the S phase, the number of colonies formed, the migratory capacity and the invasive capacity were all significantly reduced in the BMPR1B-OE+Zilurgisertib group (SMAD1 inhibitor). Compared with the BMPR1B-OE+Zilurgisertib group, the BMPR1B-OE+Zilurgisertib+SMAD2/3-OE group exhibited significantly increased S-phase proportion, colony formation, migration and invasion. Compared with the SMAD2/3-OE group, the BMPR1B-OE+Zilurgisertib+SMAD2/3-OE + IN-1 group (EGR1 inhibitor) showed significant reductions in S-phase proportion, colony formation, migration and invasion. Compared with the IN-1 group, the BMPR1B-OE+Zilurgisertib+SMAD2/3-OE + IN-1 + PDL1-OE group exhibited significantly enhanced S-phase proportion, colony formation, migration and invasion. Finally, compared with the PDL1-OE group, the BMPR1B-OE+Zilurgisertib+SMAD2/3-OE + IN-1 + PDL1-OE+XBP1-KD group showed significant reductions in all these parameters (Fig. 8 and Fig. 9). The original blots and raw data of this study were provided in Supplementary File 2 and Supplementary File 3, respectively.

A: Flow cytometry analysis of OSCC cell cycle;

B: Colony formation assay for OSCC cell proliferation;

C: Wound healing assay for OSCC cell migration;

D: Transwell assay for OSCC cell migration and invasion. Data are presented as mean ± SD, n = 3 per group. $^{ns}p > 0.05$, $*p < 0.05$.

A: Colony formation assay for Ca9-22 cell proliferation in the following groups: NC group, BMPR1B-OE group, BMPR1B-OE+Zilurgisertib group, BMPR1B-OE+Zilurgisertib+SMAD2/3-OE group, BMPR1B-OE+Zilurgisertib+SMAD2/3-OE + IN-1 group, BMPR1B-OE+Zilurgisertib+SMAD2/3-OE + IN-1 + PDL1-OE group, and BMPR1B-OE+Zilurgisertib+SMAD2/3-OE + IN-1 + PDL1-OE+XBP1-KD group.

B: Transwell assay for Ca9-22 cell migration (upper panels) and invasion (lower panels) in each group. Data are presented as mean ± SD, n = 3 per group. $^{ns}p > 0.05$, $*p < 0.05$.

3 Discussion

Oral squamous cell carcinoma (OSCC) is one of the most frequent malignant tumors in the head and neck region[6]. The main reasons for poor prognosis of the patient are its high invasiveness, high recurrence rate and tendency to metastasize to lymph nodes. Recent research consensus indicates that the malignant progression of the tumour is related not only to the intrinsic characteristics of the tumour cells themselves but also closely to the complex microenvironment in which they are situated[7]. Here, we used single-cell transcriptomics analysis to systematically map the cellular landscape of the OSCC tumour microenvironment for the first time, and identified eight major functional cell clusters. The macrophage population in tumour tissue presented a significant shift towards M2-type polarisation and highly heterogeneous developmental trajectories, providing evidence at the cellular level for a deeper

understanding of the oncogenic functions of tumour-associated macrophages (TAMs)[8]. Tumour-associated macrophages (TAMs) represent the most abundant immune cell type in the tumour microenvironment (TME) and can greatly influence tumour outcome depending on their state of polarisation. M2-type TAMs, among them, are the accelerators of tumour immune evasion and metastasis by secreting immunosuppressive cytokines, promoting angiogenesis and degrading extracellular matrix[9, 10]. Therefore, it is important to clarify the specific regulatory mechanisms of polarisation of TAMs to M2 phenotype for developing novel immunotherapy strategies for oral squamous cell carcinoma. Here, we use single-cell transcriptomic sequencing and bioinformatic analysis to reveal a novel tumour-cell regulation pathway of TAMs through the BMPR1B/BMPR2-SMAD1/EGR1/PD-L1/XBP-1 signalling axis, providing a molecular-level explanation for the formation of the immunosuppressive microenvironment and malignant progression in oral squamous cell carcinoma.

Traditionally the bone morphogenic protein (BMP) signalling pathway has been identified as playing a key role in embryonic development, bone formation and tissue repair[11]. Bone morphogenetic protein receptor 1B (BMPR1B) is a typical type I BMP receptor that transduces the classical downstream signalling by phosphorylating SMAD1/5/8 proteins upon ligand binding[12]. However, the single-cell transcriptomic analysis performed in this study revealed a specific upregulation of BMPR2 and exosome-related proteins (CD9, TSG101) in oral squamous cell carcinoma (OSCC) cells, while BMPR1B is predominantly expressed on TAMs. This spatial separation of BMP signaling components—BMPR2 in tumor cells and BMPR1B in macrophages—reveals a novel intercellular signaling axis: tumor cells package BMPR2 into exosomes and deliver it to TAMs, where it forms a functional heterodimeric complex with BMPR1B to initiate downstream SMAD signaling. This mechanism transforms the traditionally cell-autonomous BMP signaling into a paracrine tumor-macrophage communication mode, which is of profound biological significance. This indicates that cancer cells may exploit essential molecules within developmental pathways during the malignant transformation of OSCC, giving them new pro-tumour biological functions, which is called functional reprogramming. In this case, OSCC cells exploit the BMP signaling system not for their own autonomous growth signaling, but to remotely reprogram TAMs into an immunosuppressive M2 phenotype via exosomal delivery of BMPR2. Our study reveals a novel mechanism of pro-tumor action of BMP signaling in OSCC, which operates through intercellular communication rather than cell-autonomous signaling. Specifically, OSCC cells upregulate exosome biogenesis and package BMPR2 into exosomes. Upon delivery to TAMs, exosomal BMPR2 binds to and activates BMPR1B on the macrophage surface, acting as the priming signaling event that sets the molecular stage for M2 polarization. This finding fundamentally revises the traditional view that BMP receptors function exclusively in a cis-configuration within the same cell, and instead establishes a trans-cellular receptor complementation model in which the tumor provides the type II receptor (BMPR2) via exosomes while the macrophage contributes the type I receptor (BMPR1B), together reconstituting a functional BMP signaling unit on the TAM surface. Interestingly, bioinformatic analysis indicated that the expression of BMPR2 (predominantly in tumor cells) promotes the function of BMPR1B (predominantly in TAMs), supporting the trans-cellular model proposed here. BMPR2 is a type II BMP receptor that normally complexes heterodimerically with BMPR1B to transduce signals[13]. However, unlike the

classical cis-signaling within the same cell, our data demonstrate that in OSCC, BMPR2 (produced by tumor cells) and BMPR1B (expressed on macrophages) function in trans across cell types via exosome-mediated delivery. This trans-cellular signaling ensures that macrophages without endogenous BMPR2 overexpression can still respond robustly to tumor-derived signals[14]. This state not only enhances the sensitivity of tumour cells to autocrine or paracrine BMP signals in the microenvironment, but also provides the material basis for the subsequent delivery of BMPR2 protein to TAMs through exosomes, which is the novel intercellular interaction mode in this study. Exosomes are nanoscale extracellular vesicles that are important carriers of intercellular communication in the tumor microenvironment[15]. In this study, the overexpression of BMPR2 in OSCC cells together with the upregulation of exosome markers CD9 and TSG101, and the predominant expression of BMPR1B on TAMs, strongly suggests exosome-mediated intercellular communication as the mechanistic basis for trans-cellular BMP signaling. This finding expands our understanding of the regulatory mechanisms of TAM polarization: tumor cells do not rely solely on soluble factor gradients but actively deliver the 'hardware component'—BMPR2 protein—via exosomes to 'reprogram' macrophages, equipping them with enhanced BMP signaling capacity through receptor complex formation. This exosome-mediated 'hardware remodelling' represents a more precise and sustained mode of intercellular communication.

The downstream signalling events uncovered here, particularly the cascading phosphorylation of SMAD proteins, are a significant contribution and challenge to classical BMP/TGF-β signalling theory highlighting the high complexity and regulatory plasticity of cellular signalling networks[16, 17]. Binding of a ligand to the BMPR1B receptor results in phosphorylation of the receptor regulated SMAD proteins (i.e. SMAD1/5/8). Phosphorylated SMAD1/5/8 enter the nucleus to regulate gene transcription[18]. SMAD2/3, meanwhile, are the primary R-SMADs in the TGF-β/activin pathway[19]. We observed that BMPR1B overexpression simultaneously increased the levels of p-SMAD1 and p-SMAD2/3, and that SMAD1 knockdown attenuated p-SMAD2/3, suggesting that SMAD1 may influence the phosphorylation of SMAD2/3 via a certain mechanism; however, the specific molecular details require further investigation. Subsequently, SMAD2/3 can up-regulate the expression of early growth response protein 1 (EGR1). The early growth response protein 1 (EGR1) is a transcription factor encoded by an immediate early gene that can respond rapidly to a variety of stimuli including growth factors, stress and hypoxia and regulates cell proliferation, differentiation and apoptosis[20, 21]. The study identifies EGR1 as the central hub of this signaling pathway, with two downstream effector branches forming a perfect positive feedback loop and a closed-loop immunosuppressive circuit. EGR1 induces expression of TGF-β which promotes binding of TGF-β to TGFβR. This in turn enhances stability of SMAD2/3. Once this circuit is activated, TAMs can sustain high SMAD2/3 phosphorylation and high EGR1 expression for a long time through autocrine TGF-β, even when upstream BMP signalling is impaired, partially consolidating their M2 phenotype. EGR1 can induce TGF-β expression and TGF-β may further activate SMAD2/3 creating a potential positive feedback loop. Future time-course experiments should test this possibility. Secondly, EGR1 directly induces expression of PD-L1, a key hub connecting this pathway to adaptive immune suppression. PD-L1 is a classic immune checkpoint molecule, which binds to PD-1 expressed on the surface of T cells, leading to T cell exhaustion. PD-1 signaling in TAMs can induce endoplasmic

reticulum stress (ERS). PD-1 signalling in T cells has been extensively studied, but the function of PD-1 signalling in myeloid cells like macrophages, especially with regard to its association with ERS, remains a relatively frontier area of research. Previous studies have shown that PD-1 signaling can inhibit macrophage phagocytosis and the production of inflammatory cytokines[22]. Endoplasmic reticulum stress activates the unfolded protein response (UPR), a major cellular response to protein folding stress. X-box-binding protein 1 (XBP-1) is an important transcription factor in the UPR pathway, the mRNA of which is spliced by the endoplasmic reticulum transmembrane protein IRE1α to encode the more transcriptionally active sXBP-1[23]. In the present study, we identified XBP-1, which is at the terminal end of this signalling pathway, as the final executor of M2 polarisation, and simultaneously driving the progression of tumour malignancy. The role of XBP-1 in promoting M2 polarisation is in line with its role in other immune cells. During differentiation of B cells into plasma cells, XBP-1 is critical for upregulation of the synthesis and secretion of secretory proteins. XBP-1 has been previously demonstrated to be involved in the IL-4/IL-13 mediated induction of M2 polarisation in macrophages. The present study displayed that XBP-1 directly upregulates the transcription of hallmark M2 macrophage molecules, including the anti-inflammatory cytokine IL-10, surface receptor CD206 and arginase 1 (Arg1). This molecularly confirms that XBP-1 is a direct transcriptional regulator that drives TAMs to acquire pro-tumour functions. More importantly, XBP-1 also upregulates the expression of cathepsin L. Cathepsin L is a lysosomal cysteine protease which degrades extracellular matrix components such as collagen and laminin, and promotes tumour invasion and metastasis in the tumour microenvironment[24, 25]. It is a clever finding that links the immunosuppressive phenotype of TAMs to their role in driving solid tumour invasion. This closes a full logical chain: OSCC cells co-opt TAMs via the BMP signalling pathway, turning them into not only immunosuppressive outposts but also agents that can erode surrounding tissues and enable metastasis. Unlike prior investigations of breast and lung cancer, where BMPR1B was found to promote the proliferation of tumour cells, this is the first study to indicate that BMPR1B acts within the microenvironment of oral squamous cell carcinoma through the regulation of TAM polarization. This observation is in line with recent studies showing the role of XBP-1 in driving M2 polarisation; however, by integrating PD-L1 and the endoplasmic reticulum stress pathway in one signalling axis, we provide a more complete picture.

In summary, this study demonstrates that OSCC cells deliver BMPR2 via exosomes to TAMs, where exosomal BMPR2 activates BMPR1B on the macrophage surface and triggers the SMAD1/EGR1/PD-L1/XBP-1 signaling cascade, thereby inducing M2 polarization and promoting OSCC progression (Fig. 10). Here we show that the tumour microenvironment remodels the polarisation direction and developmental state of macrophages at the single-cell level and also integrates and amplifies pro-tumour signals by an enhanced intercellular communication network targeting macrophages. This finding connects intracellular signal transduction in TAMs to the cellular ecological remodelling of TME, providing a more systematic perspective to understand immune regulation of OSCC. Of course, the mechanisms proposed in this study, especially the details of the SMAD protein phosphorylation cascade, need to be validated by more in-depth experiments. Furthermore, large cohort studies are required to study the correlation of expression of signature molecules of this signalling pathway with staging,

prognosis and treatment response of patients with oral squamous cell carcinoma. In summary, this newly discovered signaling pathway not only enriches our understanding of the complexity of tumor immunology in oral squamous cell carcinoma, but also provides new ideas for the development of accurate and effective combination immunotherapy strategies, bringing new hope for the improvement of the prognosis of patients with oral squamous cell carcinoma.

Declarations

Competing Interests Statement

The authors declare that they have no competing interests.

Funding

The authors received no funding for this work.

Ethics declarations

Ethics Committee of Academic Committee of Hebei North University provided full approval for this research(No.HBNU2023041022771).

Data availability statement

The raw measurements are available in the supplementary files

Author contributions

Designing the experiment: FW, ZZ, ML, FX; Performed the experiments: FW, ZZ, ML, YY, FX; Analyzing the data: ZZ, ML, YY; Prepared the figures and/or tables: ZZ, YY; Drafted the work or revised it critically for important content: FW, ZZ, ML, YY, FX.

References

1. Bugshan A, Farooq I. Oral squamous cell carcinoma: metastasis, potentially associated malignant disorders, etiology and recent advancements in diagnosis. F1000Res. 2020;9:229. Epub 2020/05/14. doi: 10.12688/f1000research.22941.1. PubMed PMID: 32399208; PubMed Central PMCID: PMCPMC7194458.
2. Bilotta MT, Antignani A, Fitzgerald DJ. Managing the TME to improve the efficacy of cancer therapy. Front Immunol. 2022;13:954992. Epub 2022/11/08. doi: 10.3389/fimmu.2022.954992. PubMed PMID: 36341428; PubMed Central PMCID: PMCPMC9630343.
3. Vitale I, Manic G, Coussens LM, Kroemer G, Galluzzi L. Macrophages and Metabolism in the Tumor Microenvironment. Cell Metab. 2019;30(1):36-50. Epub 2019/07/04. doi: 10.1016/j.cmet.2019.06.001. PubMed PMID: 31269428.

4. Gong YM, Wang XY, He XY, Liu YF, Yu P, Chu MX, et al. Progress on the effect of FecB mutation on BMPR1B activity and BMP/SMAD pathway in sheep. Yi Chuan. 2023;45(4):295-305. Epub 2023/04/20. doi: 10.16288/j.yczz.22-366. PubMed PMID: 37077164.
5. Renault L, Patiño LC, Magnin F, Delemer B, Young J, Laissue P, et al. BMPR1A and BMPR1B Missense Mutations Cause Primary Ovarian Insufficiency. J Clin Endocrinol Metab. 2020;105(4). Epub 2019/11/27. doi: 10.1210/clinem/dgz226. PubMed PMID: 31769494.
6. Zhou J, Hu Z, Wang L, Hu Q, Chen Z, Lin T, et al. Tumor-colonized Streptococcus mutans metabolically reprograms tumor microenvironment and promotes oral squamous cell carcinoma. Microbiome. 2024;12(1):193. Epub 2024/10/06. doi: 10.1186/s40168-024-01907-9. PubMed PMID: 39369210; PubMed Central PMCID: PMCPMC11452938.
7. Hu H, Deng X, Song Q, Lv H, Chen W, Xing X, et al. Prognostic Value of the Preoperative Lymphocyte-to-C-Reactive Protein Ratio and Albumin-to-Globulin Ratio in Patients with Osteosarcoma. Onco Targets Ther. 2020;13:12673-81. Epub 2020/12/18. doi: 10.2147/ott.S287192. PubMed PMID: 33328739; PubMed Central PMCID: PMCPMC7734047.
8. Han S, Bao X, Zou Y, Wang L, Li Y, Yang L, et al. d-lactate modulates M2 tumor-associated macrophages and remodels immunosuppressive tumor microenvironment for hepatocellular carcinoma. Sci Adv. 2023;9(29):eadg2697. Epub 2023/07/19. doi: 10.1126/sciadv.adg2697. PubMed PMID: 37467325; PubMed Central PMCID: PMCPMC10355835.
9. Xu J, Ding L, Mei J, Hu Y, Kong X, Dai S, et al. Dual roles and therapeutic targeting of tumor-associated macrophages in tumor microenvironments. Signal Transduct Target Ther. 2025;10(1):268. Epub 2025/08/26. doi: 10.1038/s41392-025-02325-5. PubMed PMID: 40850976; PubMed Central PMCID: PMCPMC12375796.
10. Wang K, Zhang X, Li A, Qiao X, Xu Y. The mechanism of action and therapeutic potential of tumor-associated macrophages in tumor immune evasion. Front Immunol. 2025;16:1545928. Epub 2025/05/07. doi: 10.3389/fimmu.2025.1545928. PubMed PMID: 40330472; PubMed Central PMCID: PMCPMC12052954.
11. Liao J, Wu T, Zhang Q, Shen P, Huang Z, Wang J, et al. TGF-β/BMP signaling in skeletal biology: molecular mechanisms, regulatory networks, and therapeutic implications in development, regeneration, and disease. Bone Res. 2026;14(1):6. Epub 2026/01/14. doi: 10.1038/s41413-025-00497-y. PubMed PMID: 41530114; PubMed Central PMCID: PMCPMC12800155 publication: All the authors agree to the current state of the manuscript to be submitted to the journal.
12. Jeanpierre S, Arizkane K, Thongjuea S, Grockowiak E, Geistlich K, Barral L, et al. The quiescent fraction of chronic myeloid leukemic stem cells depends on BMPR1B, Stat3 and BMP4-niche signals to persist in patients in remission. Haematologica. 2021;106(1):111-22. Epub 2020/02/01. doi: 10.3324/haematol.2019.232793. PubMed PMID: 32001529; PubMed Central PMCID: PMCPMC7776261.
13. Yun X, Chen Z, Li F, Shen F, Zhang L, Yuan J. Exosomal BMPR2 Macromolecule Facilitates Alveolar Epithelial Cell Repair Through Functional Complex Formation with BMPR1B in Acute Lung Injury. Int

J Nanomedicine. 2025;20:7233-49. Epub 2025/06/12. doi: 10.2147/ijn.S519393. PubMed PMID: 40502982; PubMed Central PMCID: PMCPMC12154541.

14. Fernandes C, Cassiano AFB, Henrique-Silva F, Cirelli JA, de Souza EP, Coaguila-Llerena H, et al. Recombinant sugarcane cystatin CaneCPI-5 promotes osteogenic differentiation. Tissue Cell. 2023;83:102157. Epub 2023/07/15. doi: 10.1016/j.tice.2023.102157. PubMed PMID: 37451011.
15. Zhou X, Jia Y, Mao C, Liu S. Small extracellular vesicles: Non-negligible vesicles in tumor progression, diagnosis, and therapy. Cancer Lett. 2024;580:216481. Epub 2023/11/17. doi: 10.1016/j.canlet.2023.216481. PubMed PMID: 37972701.
16. Kim BG, Lee JH, Yasuda J, Ryoo HM, Cho JY. Phospho-Smad1 modulation by nedd4 E3 ligase in BMP/TGF-β signaling. J Bone Miner Res. 2011;26(7):1411-24. Epub 2011/02/11. doi: 10.1002/jbmr.348. PubMed PMID: 21308777.
17. Wrighton KH, Lin X, Feng XH. Phospho-control of TGF-beta superfamily signaling. Cell Res. 2009;19(1):8-20. Epub 2008/12/31. doi: 10.1038/cr.2008.327. PubMed PMID: 19114991; PubMed Central PMCID: PMCPMC2929013.
18. Wang S, Hu S, Wang J, Liu Y, Zhao R, Tong M, et al. Conditioned medium from bone marrow-derived mesenchymal stem cells inhibits vascular calcification through blockade of the BMP2-Smad1/5/8 signaling pathway. Stem Cell Res Ther. 2018;9(1):160. Epub 2018/06/14. doi: 10.1186/s13287-018-0894-1. PubMed PMID: 29895327; PubMed Central PMCID: PMCPMC5998505.
19. Khalil H, Kanisicak O, Prasad V, Correll RN, Fu X, Schips T, et al. Fibroblast-specific TGF-β-Smad2/3 signaling underlies cardiac fibrosis. J Clin Invest. 2017;127(10):3770-83. Epub 2017/09/12. doi: 10.1172/jci94753. PubMed PMID: 28891814; PubMed Central PMCID: PMCPMC5617658 exists.
20. Kim TY, Yeo H, Jung E, Shin SY. EGR1 interacts with p-SMAD at the endothelin-1 gene promoter to regulate gene expression in TGFβ1-stimulated IMR-90 fibroblasts. Biochem Biophys Res Commun. 2024;739:150567. Epub 2024/08/27. doi: 10.1016/j.bbrc.2024.150567. PubMed PMID: 39186868.
21. Bi JG, Zheng JF, Li Q, Bao SY, Yu XF, Xu P, et al. MicroRNA-181a-5p suppresses cell proliferation by targeting Egr1 and inhibiting Egr1/TGF-β/Smad pathway in hepatocellular carcinoma. Int J Biochem Cell Biol. 2019;106:107-16. Epub 2018/12/07. doi: 10.1016/j.biocel.2018.11.011. PubMed PMID: 30503931.
22. Jiang Z, Lim SO, Yan M, Hsu JL, Yao J, Wei Y, et al. TYRO3 induces anti-PD-1/PD-L1 therapy resistance by limiting innate immunity and tumoral ferroptosis. J Clin Invest. 2021;131(8). Epub 2021/04/16. doi: 10.1172/jci139434. PubMed PMID: 33855973; PubMed Central PMCID: PMCPMC8262501.
23. Ribeiro CM, Lubamba BA. Role of IRE1α/XBP-1 in Cystic Fibrosis Airway Inflammation. Int J Mol Sci. 2017;18(1). Epub 2017/01/12. doi: 10.3390/ijms18010118. PubMed PMID: 28075361; PubMed Central PMCID: PMCPMC5297752.
24. Peng Z, Luo XY, Li X, Li Y, Wu Y, Tian Y, et al. Cathepsin L Promotes Pulmonary Hypertension via BMPR2/GSDME-Mediated Pyroptosis. Hypertension. 2024;81(12):2430-43. Epub 2024/10/15. doi: 10.1161/hypertensionaha.124.22903. PubMed PMID: 39403807.

25. Han ML, Zhao YF, Tan CH, Xiong YJ, Wang WJ, Wu F, et al. Cathepsin L upregulation-induced EMT phenotype is associated with the acquisition of cisplatin or paclitaxel resistance in A549 cells. Acta Pharmacol Sin. 2016;37(12):1606-22. Epub 2016/11/15. doi: 10.1038/aps.2016.93. PubMed PMID: 27840408; PubMed Central PMCID: PMCPMC5309731.

Figures

Fig1

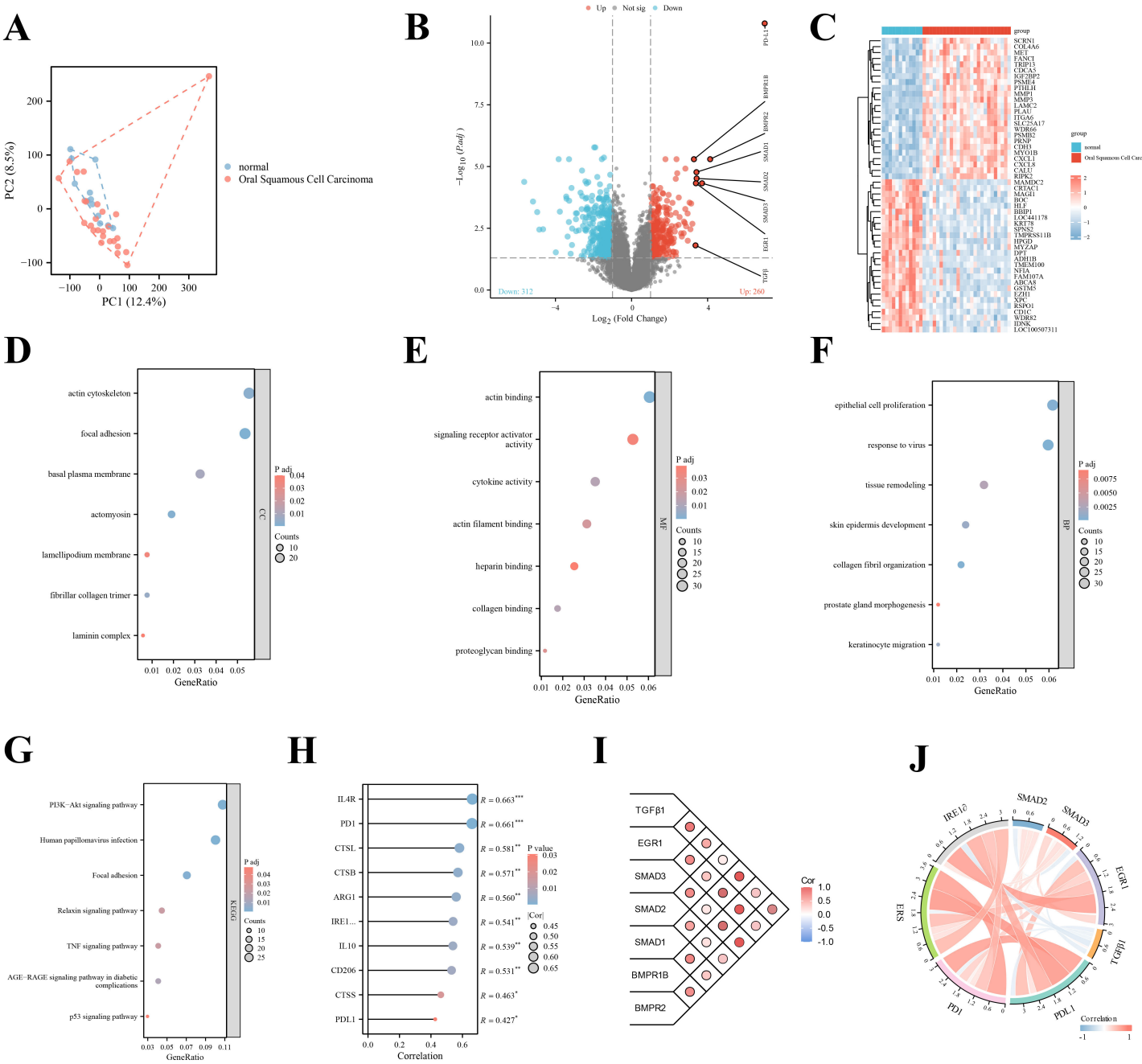


Figure 1

Single-cell transcriptome analysis.

A: UMAP expression distribution of genes;

B: Violin plot of gene expression across cell types;

C: UMAP dimensionality reduction and clustering of cell types;

D: Heatmap of gene expression by cell type.

Fig2

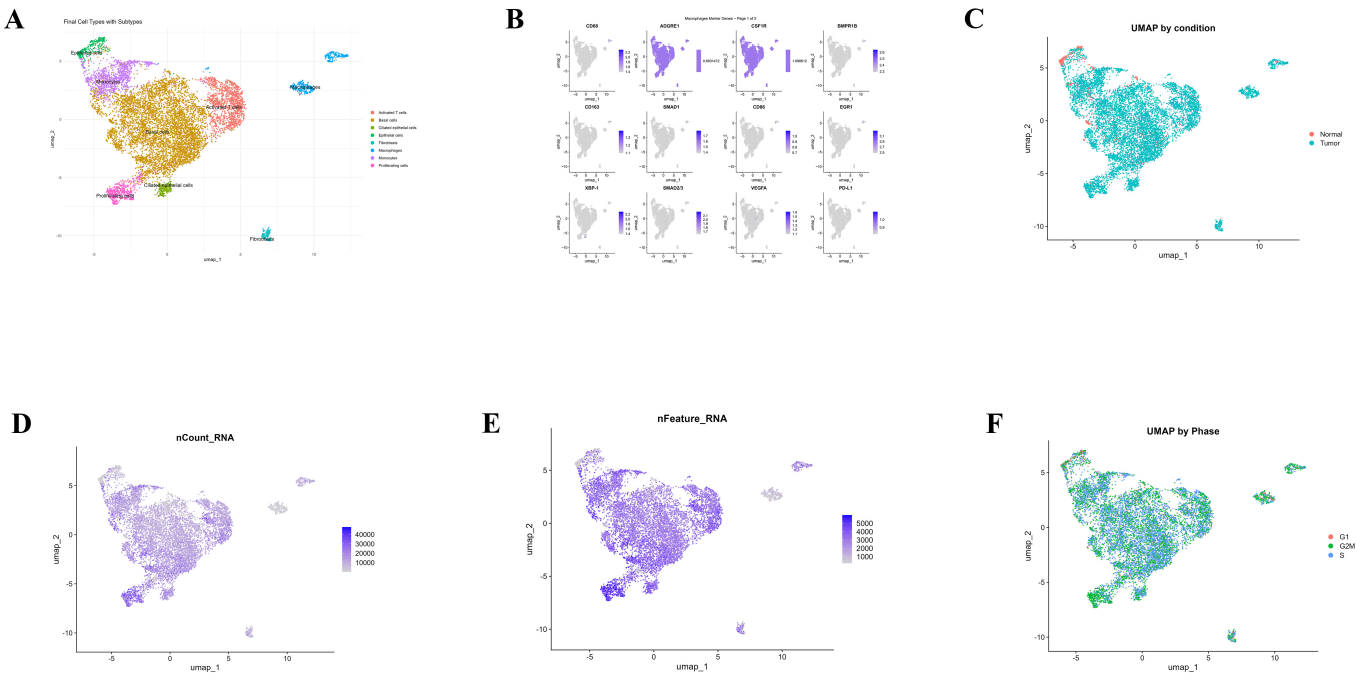


Figure 2

Construction of a single-cell transcriptomic atlas of oral squamous cell carcinoma

A: Cell type UMAP plot

B: Expression of macrophage marker genes

C: Clustering UMAP plot

D: nCount_RNA UMAP plot

E: nFeature_RNA UMAP plot

F: Cell cycle UMAP plot;

Fig3

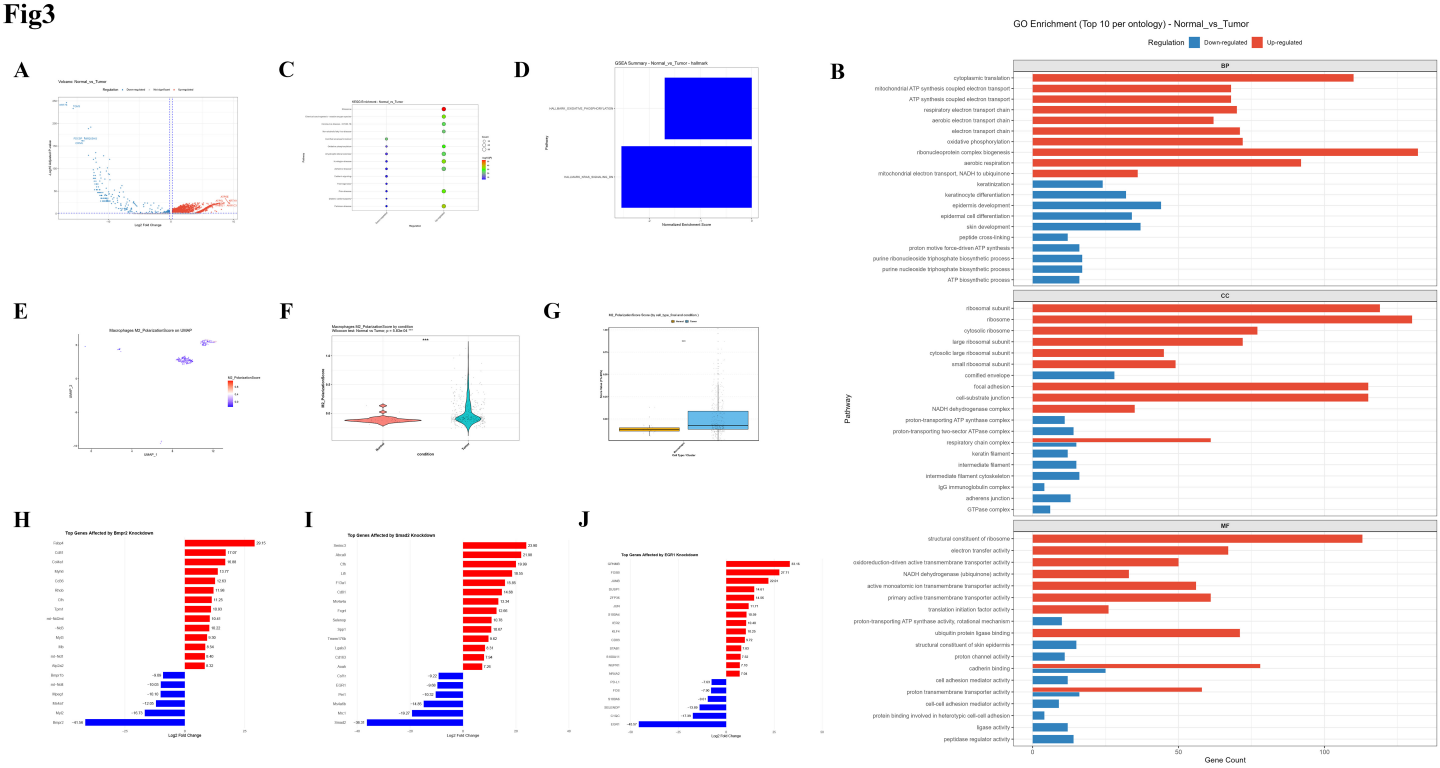


Figure 3

Functional enrichment analysis of differentially expressed genes and M2-type immunosuppressive polarisation of macrophages in oral squamous cell carcinoma

A: Volcano plot of differentially expressed genes

B: Bar chart of GO enrichment analysis

C: Bubble plot of KEGG enrichment analysis

D: Gene set enrichment analysis

E: Inter-group comparison of macrophage M2 polarisation scores

F: Violin plot comparison of macrophage M2 polarisation scores between the normal (Normal) and tumour (Tumour) groups

G: Box plot comparison of macrophage M2 polarisation scores between the normal (Normal) and tumour (Tumour) groups;

H–J: Results following virtual knockout of BMPR2, SMAD2 and EGR1.

Fig4

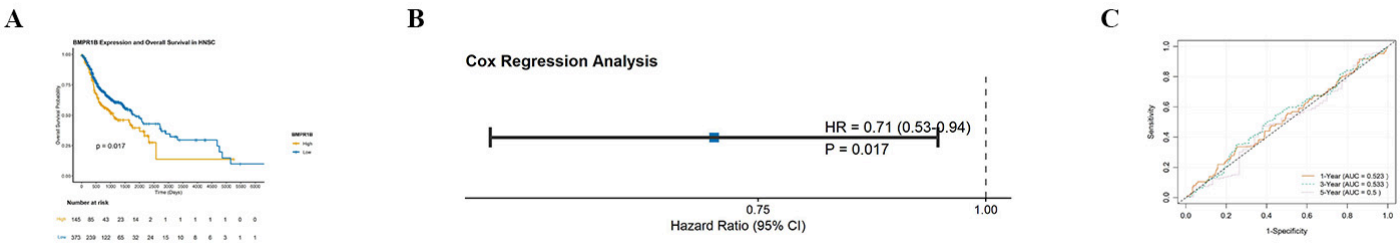


Figure 4

Association analysis between BMPR1B expression levels and overall survival in patients with head and neck squamous cell carcinoma.

A: Comparison of Kaplan–Meier overall survival curves between the high and low BMPR1B expression groups. The x-axis represents survival time (days), and the y-axis represents the probability of overall survival.

B: Forest plot of univariate Cox regression analysis showing the effect of BMPR1B expression levels on overall survival.

C: Time-dependent ROC analysis for predicting overall survival.

The predictive performance of BMPR1B expression was evaluated at 1, 3, and 5 years. The AUC values were 0.523 for 1-year, 0.533 for 3-year, and 0.500 for 5-year survival, indicating limited sensitivity and specificity.

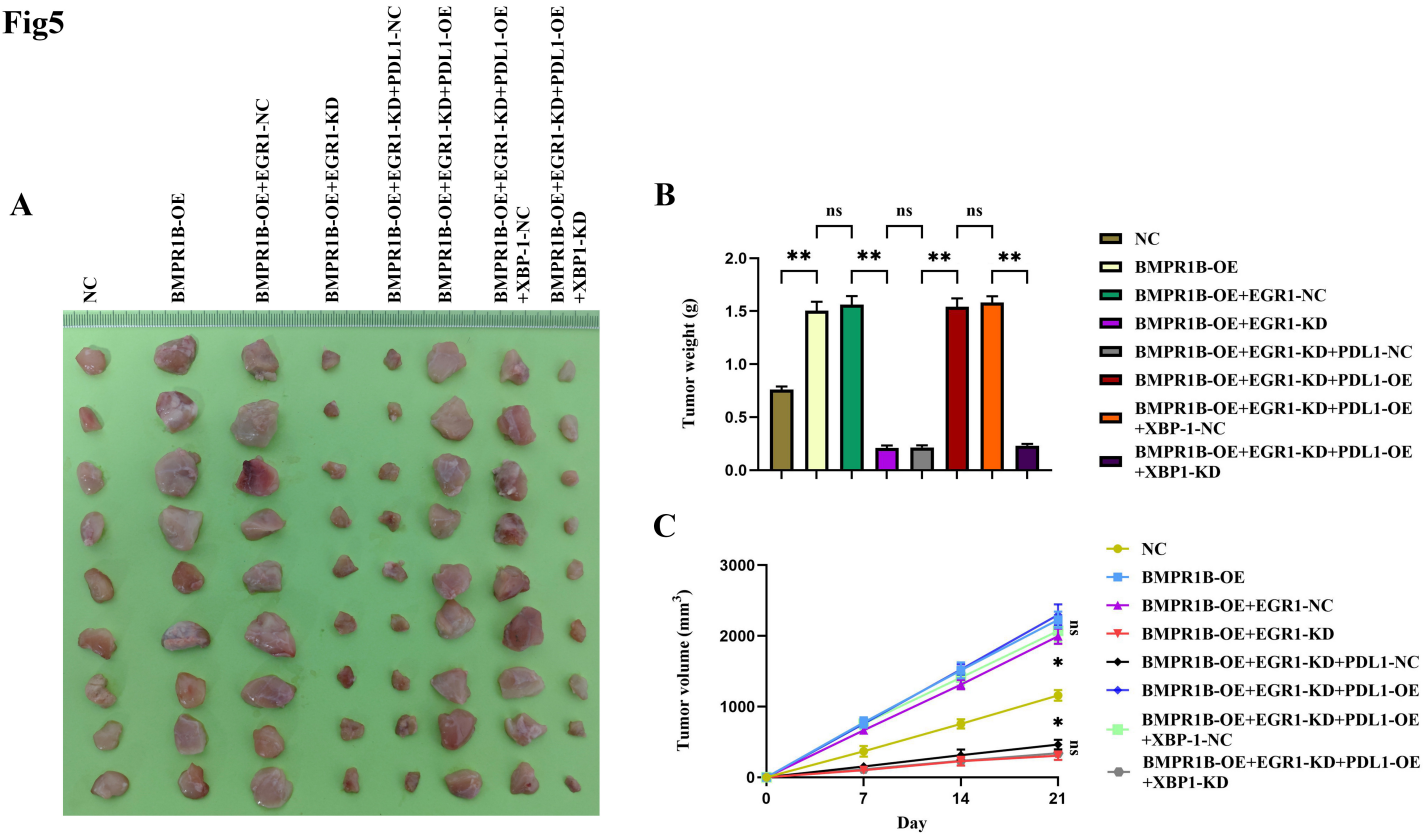


Figure 5

Activation of BMPR1B signaling in TAMs promotes OSCC tumor growth in mice via the EGR1/PD-L1/XBP-1 pathway.

A: Representative images of subcutaneous tumors from the indicated groups: NC group, BMPR1B-OE group, BMPR1B-OE+EGR1-NC group, BMPR1B-OE+EGR1-KD group, BMPR1B-OE+EGR1-KD+PDL1-NC group, BMPR1B-OE+EGR1-KD+PDL1-OE group, BMPR1B-OE+EGR1-KD+PDL1-OE+XBP-1-NC group, and BMPR1B-OE+EGR1-KD+PDL1-OE+XBP-1-KD group.

B: Statistical analysis of tumor weight (g) in each group.

C: Tumor volume growth curves measured at indicated time points (Days 0, 7, 14, 21).

Data are presented as mean ± SD, n = 9 per group. $^{ns}p > 0.05$, $*p < 0.05$.

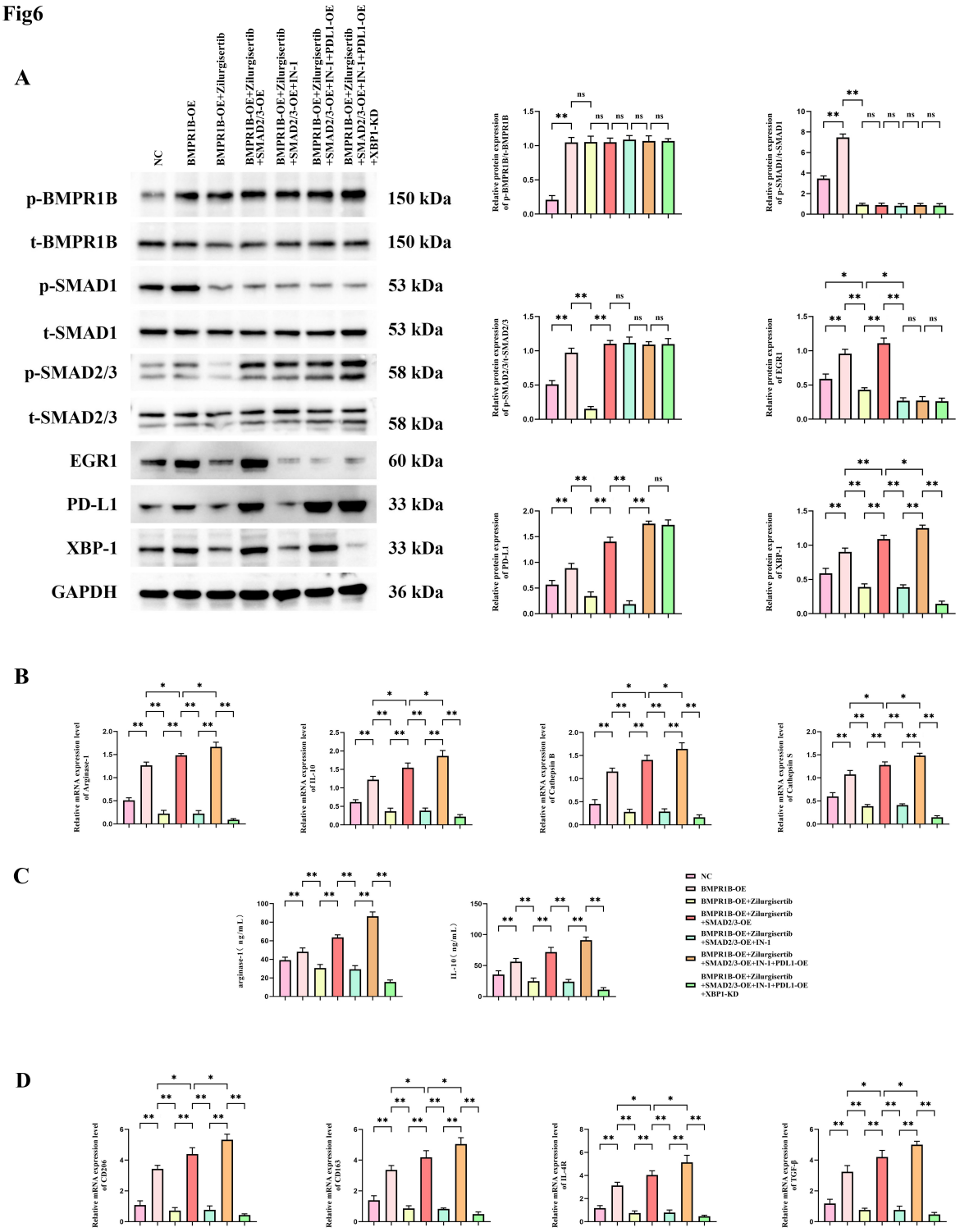


Figure 6

BMPR1B induces M2 polarization.

A: Western blot detection of p-BMPR1B, p-SMAD1, p-SMAD2/3, EGR1, PD-L1, and XBP-1 expression in the following groups: NC group, BMPR1B-OE group, BMPR1B-OE+Zilurgisertib group, BMPR1B-OE+Zilurgisertib+SMAD2/3-OE group, BMPR1B-OE+Zilurgisertib+SMAD2/3-OE+IN-1 group, BMPR1B-

OE+Zilurgisertib+SMAD2/3-OE+IN-1+PDL1-OE group, and BMPR1B-OE+Zilurgisertib+SMAD2/3-OE+IN-1+PDL1-OE+XBP1-KD group;

B: Q-PCR detection of arginase-1, IL-10, Cathepsin B and Cathepsin S levels in each group;

C: ELISA detection of arginase-1 and IL-10 levels in each group.

D: Q-PCR detection of CD206, CD163, IL-4R and TGF-β levels. Data are presented as mean ± SD, n = 3 per group. $^{ns}p > 0.05$, *p < 0.05.

Fig7

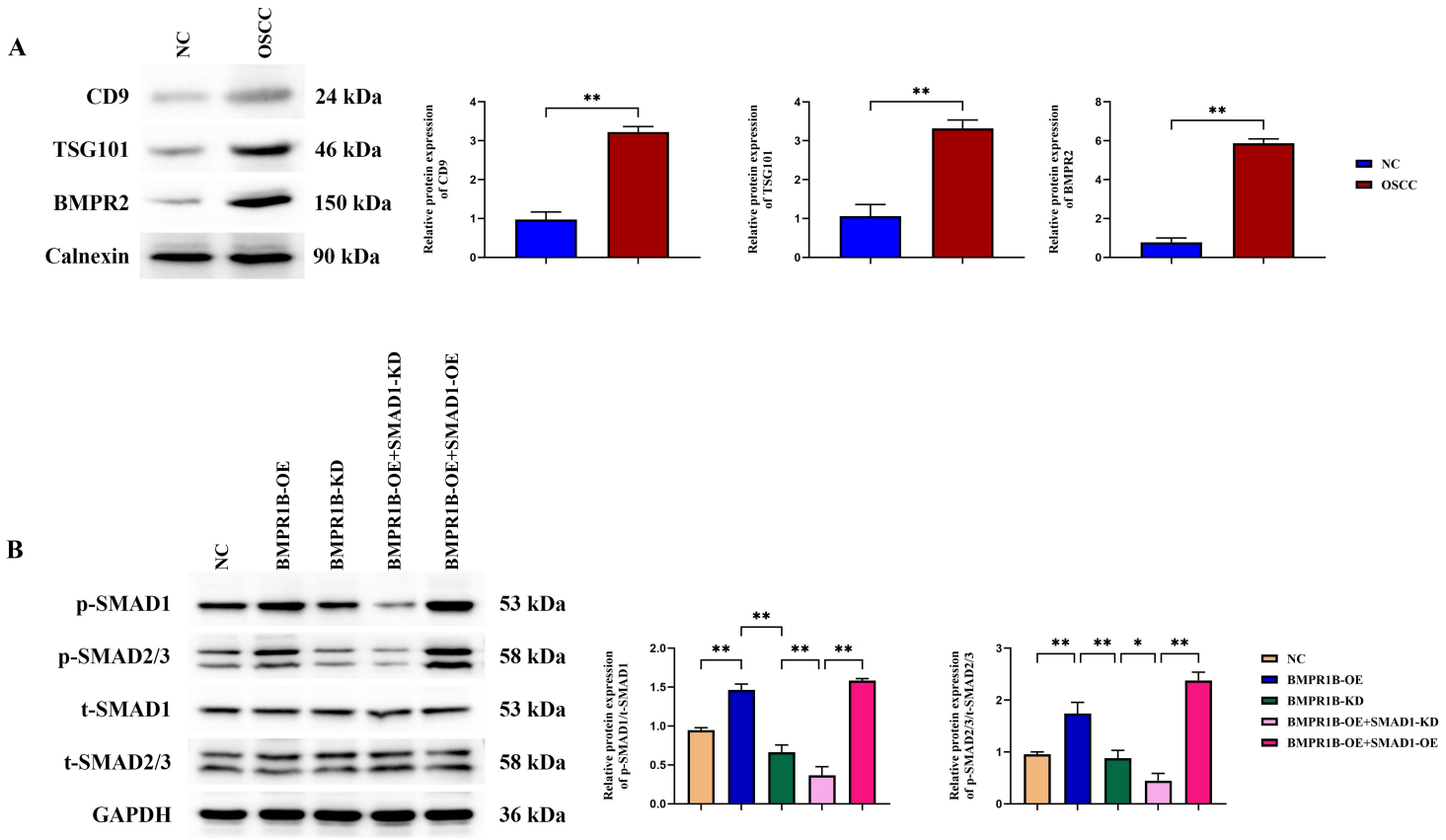


Figure 7

BMPR1B regulates SMAD signaling and exosome-related protein expression in OSCC and TAMs.

A: Western blot detection of CD9, TSG101, and BMPR2 expression in NC (normal oral cells) and OSCC (Ca9-22 cells) groups, and BMPR2 protein in exosomes isolated from Ca9-22 cell culture supernatant with or without prior BMPR2 knockdown (si-BMPR2) compared to si-NC control. Data are presented as mean ± SD, n = 3 per group.

B: Western blot detection of p-SMAD1, t-SMAD1, p-SMAD2/3, and t-SMAD2/3 expression in the following groups: NC group, BMPR1B-OE group, BMPR1B-KD group, BMPR1B-OE+SMAD1-KD group, and BMPR1B-

OE+SMAD1-OE group. Data are presented as mean ± SD, n = 3 per group. $^{ns}p > 0.05$, *p < 0.05.

Fig8

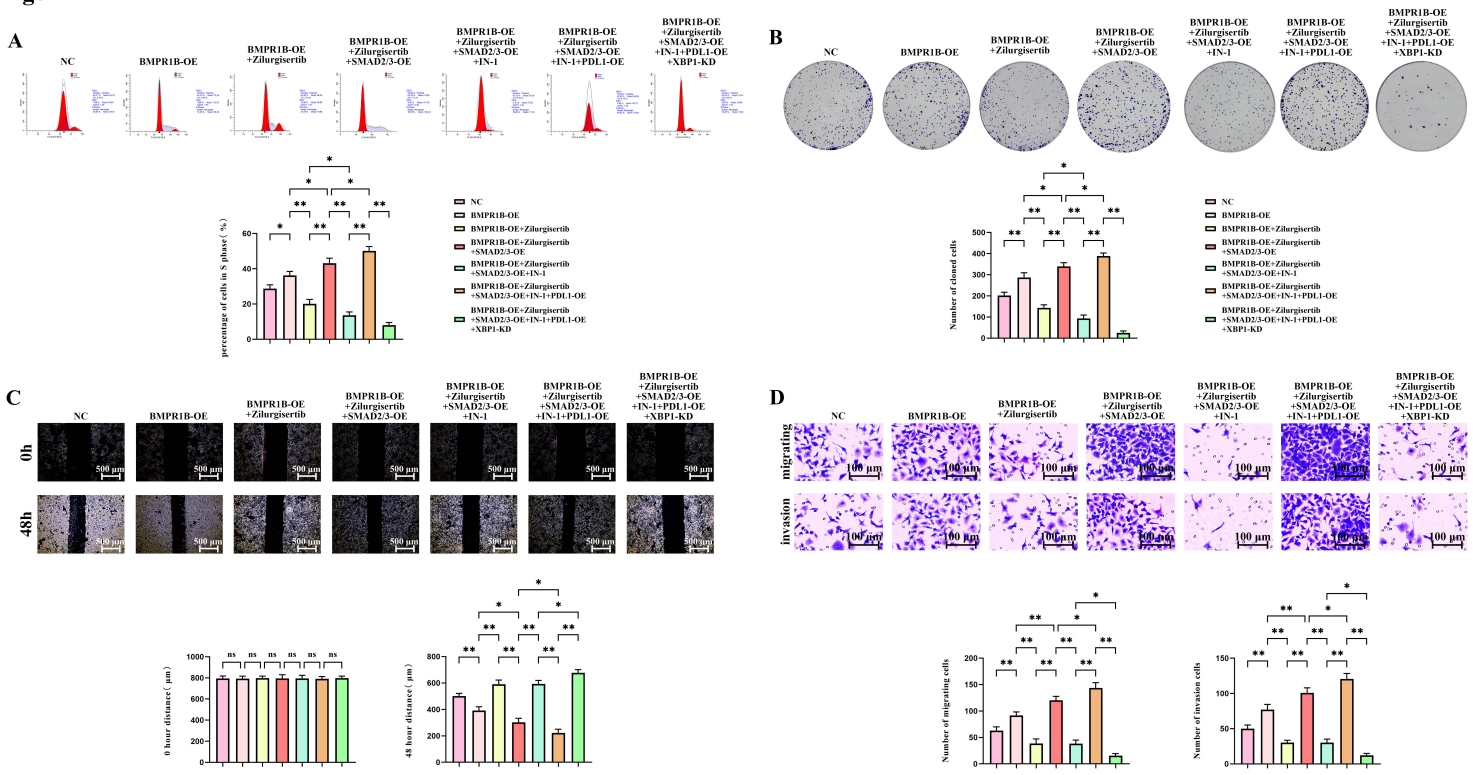


Figure 8

BMPR1B signaling in TAMs promotes OSCC cell proliferation, migration, and invasion.

A: Flow cytometry analysis of OSCC cell cycle;

B: Colony formation assay for OSCC cell proliferation;

C: Wound healing assay for OSCC cell migration;

D: Transwell assay for OSCC cell migration and invasion. Data are presented as mean ± SD, n = 3 per group. $^{ns}p > 0.05$, *p < 0.05.

Fig9

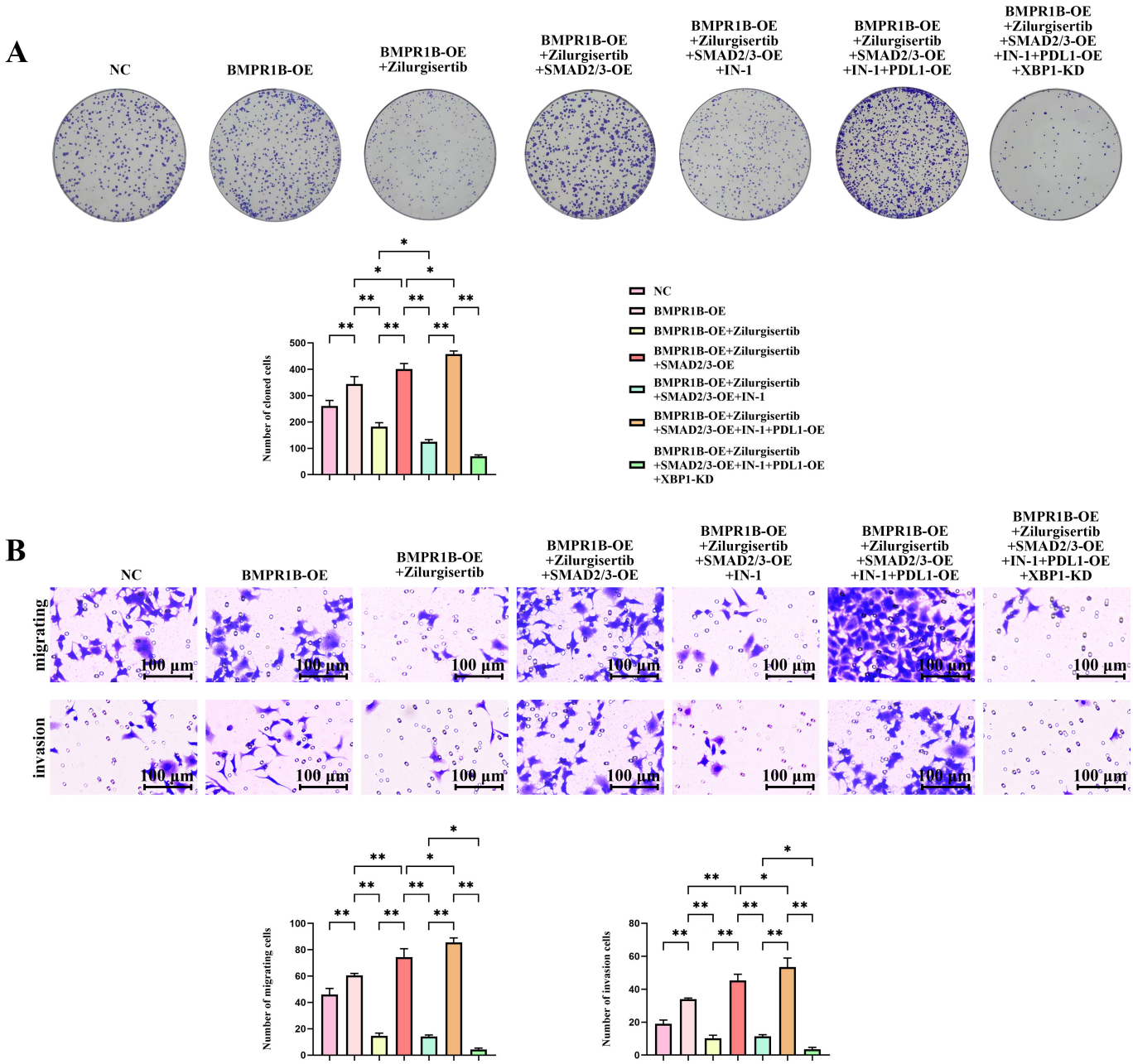


Figure 9

BMPR1B signaling promotes OSCC cell proliferation, migration, and invasion in an indirect co-culture system.

A: Colony formation assay for Ca9-22 cell proliferation in the following groups: NC group, BMPR1B-OE group, BMPR1B-OE+Zilurgisertib group, BMPR1B-OE+Zilurgisertib+SMAD2/3-OE group, BMPR1B-OE+Zilurgisertib+SMAD2/3-OE+IN-1 group, BMPR1B-OE+Zilurgisertib+SMAD2/3-OE+IN-1+PDL1-OE group, and BMPR1B-OE+Zilurgisertib+SMAD2/3-OE+IN-1+PDL1-OE+XBP1-KD group.

B: Transwell assay for Ca9-22 cell migration (upper panels) and invasion (lower panels) in each group. Data are presented as mean ± SD, n = 3 per group. $^{ns}p > 0.05$, $^{*}p < 0.05$.

Fig10

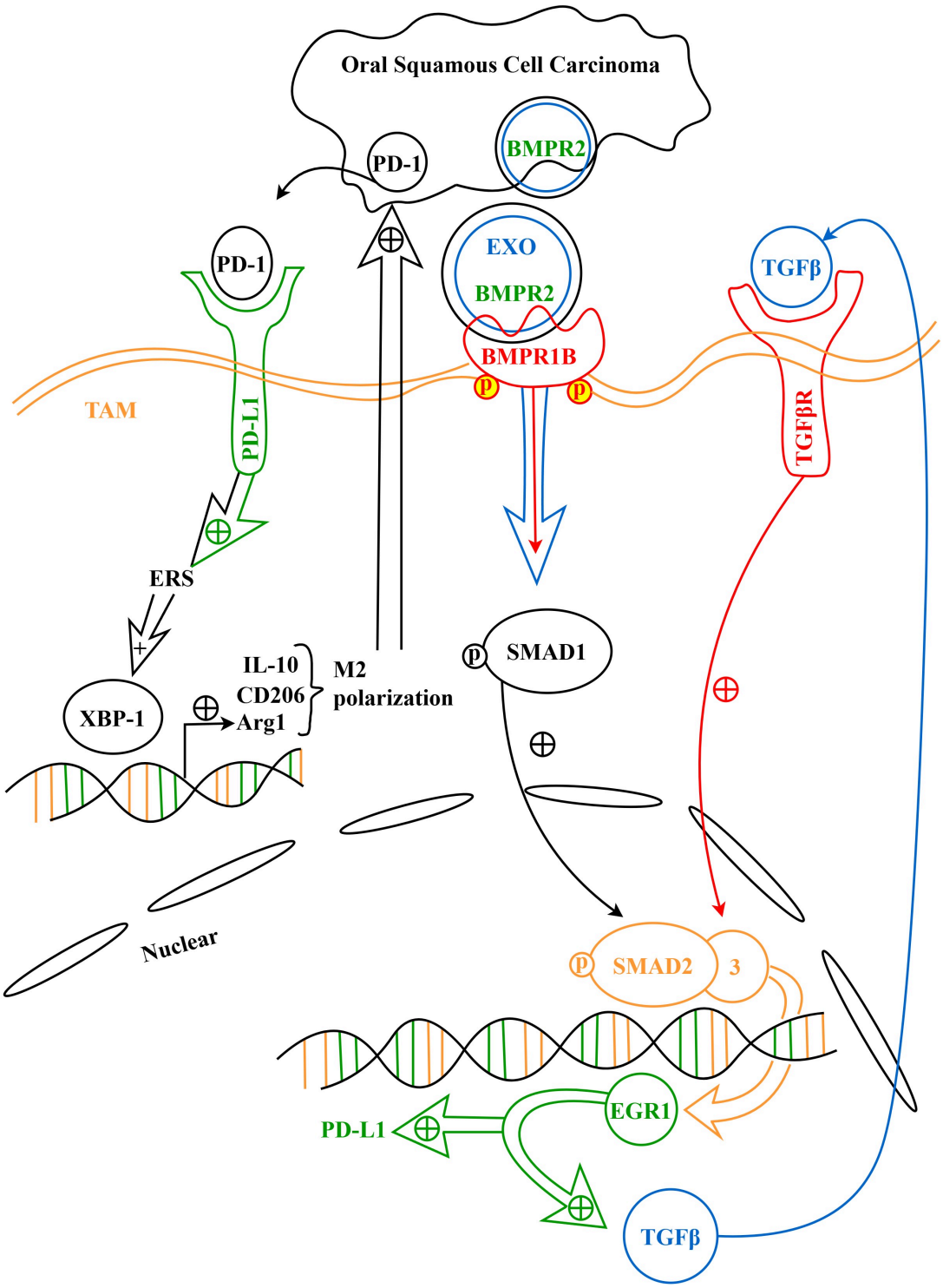


Figure 10

OSCC cells upregulate exosome biogenesis and package BMPR2 into exosomes. Exosomal BMPR2 is delivered to TAMs, where it forms a functional complex with BMPR1B on the macrophage surface, activating the SMAD1/EGR1/PD-L1/XBP-1 signaling cascade, thereby inducing M2 polarization and promoting oral squamous cell carcinoma progression.

Supplementary Files

This is a list of supplementary files associated with this preprint. Click to download.

- Supplementaryfile1.docx
- Supplementaryfile3.xlsx
- figs1.jpg
- Supplementaryfile2.pdf
- Gelsandblotsimages.pdf